Nonlinear relationship between ER Ca^{2+} depletion versus induction of the unfolded protein response, autophagy inhibition, and cell death

Paula Szalai[a,e], Jan B. Parys[b], Geert Bultynck[b], Søren Brøgger Christensen[c], Poul Nissen[d,e], Jesper V. Møller[f], and Nikolai Engedal[a,*]

[a] Centre for Molecular Medicine Norway (NCMM), Nordic EMBL Partnership for Molecular Medicine, University of Oslo, Norway

[b] KU Leuven, Laboratory of Molecular and Cellular Signaling, Department of Cellular and Molecular Medicine and Leuven Kanker Instituut (LKI), Leuven, Belgium

[c] Department of Drug Design and Pharmacology, University of Copenhagen, Denmark.

[d] Centre for Membrane Pumps in Cells and Disease (Pumpkin), Danish Research Foundation, Aarhus, Denmark

[e] Danish Research Institute of Translational Neuroscience (DANDRITE), Nordic EMBL Partnership for Molecular Medicine, Department of Molecular Biology and Genetics, Aarhus, Denmark,

[f] Department of Biomedicine, Aarhus University, Aarhus, Denmark

***Correspondence:** Nikolai Engedal, Centre for Molecular Medicine Norway (NCMM), Nordic EMBL Partnership for Molecular Medicine, University of Oslo, P.O. Box 1137 Blindern, N-0318 Oslo, Norway; Tel. (+47) 22840765; Fax. (+47) 22840598; Email: k.n.engedal@ncmm.uio.no

Highlights

- Depletion of the bulk of ER Ca^{2+} does not induce the unfolded protein response
- Cells can tolerate sustained depletion of ~ all releasable ER Ca^{2+} for several days
- Depletion of the bulk of ER Ca^{2+} does not limit bulk autophagy
- Partial depletion of ER Ca^{2+} is sufficient to reduce cell proliferation
- Cytotoxic effects require extreme ER Ca^{2+} depletion or ER subdomain Ca^{2+} depletion

Graphical abstract - Szalai et al., 2018. Cell Calcium

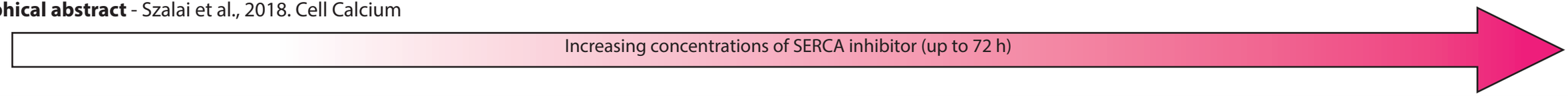

A

ER Ca^{2+} homeostasis

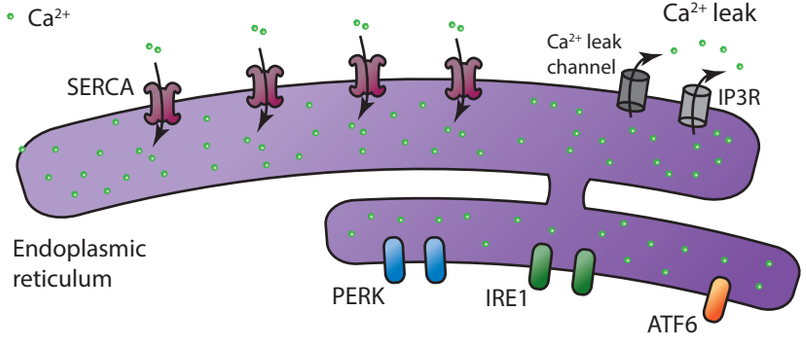

normal cell functions

B

sustained depletion of the bulk of ER Ca^{2+}

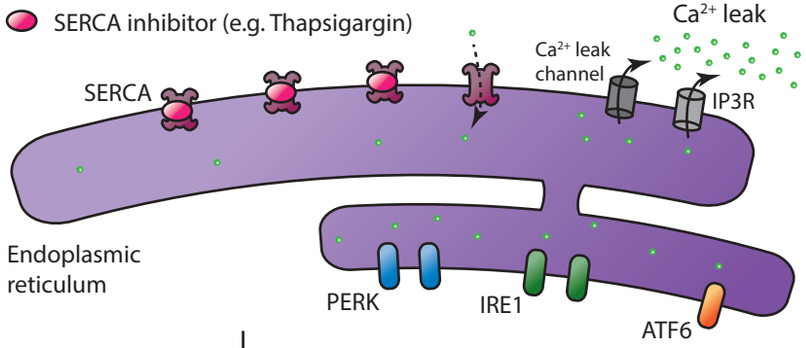

cell proliferation

C

extreme ER Ca^{2+} depletion
or
Ca^{2+} depletion of ER subdomain

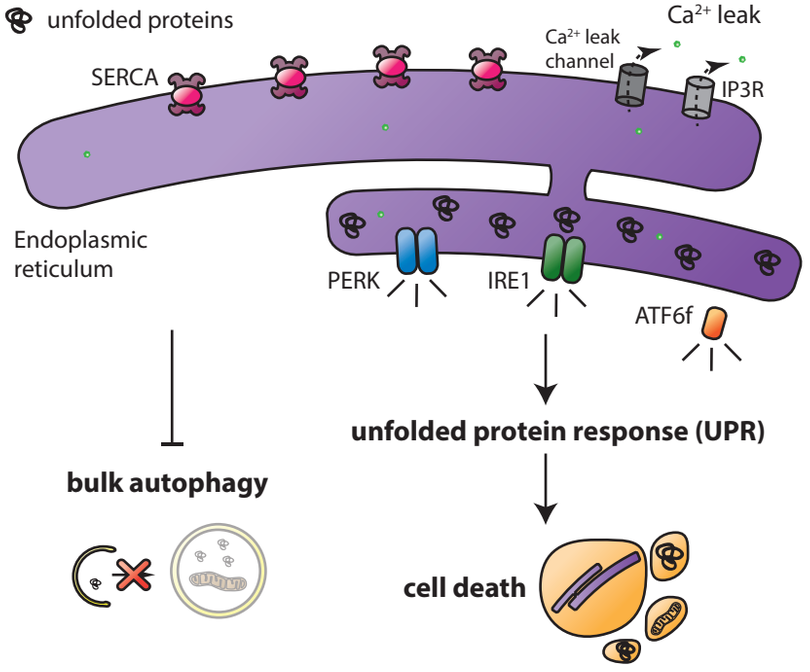

Abstract

Endoplasmic reticulum (ER) Ca^{2+} depletion activates the unfolded protein response (UPR), inhibits bulk autophagy and eventually induces cell death in mammalian cells. However, the extent and duration of ER Ca^{2+} depletion required is unknown. We instigated a detailed study in two different cell lines, using sarco/endoplasmic reticulum Ca^{2+}-ATPase (SERCA) inhibitors to gradually reduce ER Ca^{2+} levels in a controlled manner. Remarkably, UPR induction (as assessed by expression analyses of UPR-regulated proteins) and autophagy inhibition (as assessed by analyses of effects on starvation-induced bulk autophagy) required substantially higher drug concentrations than those needed to strongly decrease total ER Ca^{2+} levels. In fact, even when ER Ca^{2+} levels were so low that we could hardly detect any release of Ca^{2+} upon challenge with ER Ca^{2+} purging agents, UPR was not induced, and starvation-induced bulk autophagy was still fully supported. Moreover, although we observed reduced cell proliferation at this very low level of ER Ca^{2+}, cells could tolerate prolonged periods (days) without succumbing to cell death. Addition of increasing concentrations of extracellular EGTA also gradually depleted the ER of Ca^{2+}, and, as with the SERCA inhibitors, EGTA-induced activation of UPR and cell death required higher EGTA-concentrations that those needed to strongly reduce ER Ca^{2+} levels. We conclude that ER Ca^{2+} depletion-induced effects on UPR, autophagy and cell death require either an extreme general depletion of ER Ca^{2+} levels, or Ca^{2+} depletion in areas of the ER that have a higher resistance to Ca^{2+} drainage than the bulk of the ER.

Keywords:

ER Ca^{2+} depletion; unfolded protein response; thapsigargin; SERCA; cell death; autophagy

Abbreviations:

AUC, area under the curve; EpoTg, thapsigargin epoxide; ER, endoplasmic reticulum; LDH, lactate dehydrogenase; PI, propidium iodide; SERCA, sarco/endoplasmic reticulum Ca^{2+}-ATPase; SOCE, store-operated calcium entry; Tg, thapsigargin; UPR, unfolded protein response

1. Introduction

The endoplasmic reticulum (ER) is the major intracellular calcium store in the cell, and can harbour thousands-fold higher Ca^{2+} concentrations than those found in the cytosol. The concentration gradient is maintained by luminal Ca^{2+}-binding proteins and the ATP-driven Ca^{2+} pump SERCA, which drives cytosol-to-ER Ca^{2+} transport [1]. High intra-luminal calcium levels are crucial for Ca^{2+}-initiated signalling events, involved in numerous physiological processes. Additionally, Ca^{2+} is required for many ER functions, e.g. protein folding, modification, sorting, and quality control [2]. Likely for these reasons, cells are very sensitive to ER Ca^{2+} depletion, which induces ER stress and the unfolded protein response (UPR), and inhibits the lysosomal degradative process macroautophagy, hereafter referred to as autophagy [3, 4]. Moreover, sustained UPR leads to apoptotic cell death [4-9].

ER stress is defined as the overload of ER folding capacity, caused by abnormal accumulation of unfolded proteins. The stress is sensed by the ER transmembrane proteins PERK, IRE1, and ATF6, which together initiate the UPR – an intracellular signalling response that activates a transcriptional program aimed at alleviating the stress [2, 10, 11]. Autophagy has been suggested to contribute to alleviate the stress by ridding the cells of misfolded and aggregated proteins [12]. However, ER Ca^{2+} depletion has a dominant effect to block autophagy in a manner that does not involve the UPR [3]. Another way that the UPR attempts to alleviate ER stress is by enhancing the expression of ER-resident chaperones and foldases. One of the chaperones, GRP78/BiP, is a master regulator of the UPR, since it under non-stressed conditions keeps the UPR initiators inactive via direct interaction [13-17]. Upon ER Ca^{2+} depletion, protein folding and sorting is disturbed [18-21], because the activities of ER-resident chaperones, foldases, and post-translational modifiers depend on Ca^{2+} [2, 22]. This leads to accumulation of unfolded proteins, which, in turn, bind to and release BiP from the UPR initiators [13-15, 17], resulting in UPR activation.

The importance of understanding the cellular consequences of lowered ER Ca^{2+} levels, and its relation to the UPR, is highlighted by observations that a number human pathologies, including diabetes, cancer, viral infection, cardiovascular and neurological diseases are characterized by reduced ER Ca^{2+} levels and enhanced UPR [23-30]. However, most of the current knowledge of the association between decreases in ER Ca^{2+} levels versus induction of UPR and cell death, and effects on autophagy, is based on the use of ER Ca^{2+}-purging drugs at concentrations that give a rapid and extreme depletion of ER Ca^{2+} [31-39]. Thus, the connection between the extent, as well as the duration of ER Ca^{2+} depletion versus UPR induction, cell death, and autophagy inhibition is unknown.

To address these unanswered questions, we have here used SERCA inhibitors at a range of concentrations and time points in two commonly used cancer cell lines, to systematically determine cellular effects of gradual ER Ca^{2+} depletion. Surprisingly, we find that cells can tolerate strong and sustained decreases in ER Ca^{2+} levels without showing any signs of UPR induction, autophagy inhibition or cell death. Instead, these type of cellular responses to ER

Ca^{2+} depletion appear to require either an extreme overall ER Ca^{2+} depletion, or Ca^{2+} depletion in areas of the ER that are more resistant to Ca^{2+} drainage than other parts of the ER.

2. Materials and methods

2.1 Cell culture and compounds

PC3 cells (ATCC, CRL-1435) and LNCaP cells (ATCC, CRL-1740) were maintained in RPMI 1640 (Thermo Fisher Scientific, 21875091) containing 10% FBS (Sigma, F7524 batch BCBT0730), and cultured at 37°C in a humidified 5% CO_2 incubator. In experiments with EGTA, cells were incubated in calcium-free DMEM (Thermo Fisher Scientific, 21068028) with 10% FBS. Thapsigargin epoxide (EpoTg) was prepared as described previously [40]. Other compounds were: Thapsigargin (Sigma, T9033), A23187 (Sigma, T9033), ATP (Sigma, A6419), Ionomycin (Sigma, I9657), Bafilomycin A1 (Enzo, BML-CM110), EGTA (Sigma, E8145), Z-VAD-FMK (Adooq Bioscience, A12373), and Propidium Iodide (Merck, 537059).

2.2 Cell death and cell confluency assessment

Cell death was assessed as previously described [4, 41]. Briefly, cells were seeded in triplicates in 96-well plates and grown to ~70% confluency. Treatments were added along with 2.5 µg/ml (final concentration) propidium iodide, and the IncuCyte ZOOM imaging system (Essenbio) was used for live-cell phase-contrast and fluorescence imaging, acquiring 3 images from each well every 3 h. The integrated software was used to calculate ratio of red fluorescence- to total cell confluency, as previously described [4, 41], and relative cell death was plotted as a function of time, normalized to the average ratio from each experiment when indicated. Cell confluency was calculated from the phase-contrast images at each time point using the IncuCyte ZOOM software.

2.3 Cell viability assessment

Cell viability was assessed by the CellTiter 96 AQ_{ueous} One Solution assay (Promega, G3581). Cells were seeded in 96-well plates and grown to ~70% confluency, followed by treatment with EpoTg or Tg for 44 h. Thereafter, 20 µl CellTiter 96 AQ_{ueous} One Solution was added to each well, and the incubation was continued for 2 h at 37°C in a humidified 5% CO_2 incubator. Absorbance was recorded at 450 nm using a Tecan Infinite F200 plate reader. Background absorbance was recorded from wells containing cell culture medium and CellTiter 96 AQ_{ueous} One Solution, but no cells.

2.4 Cytosolic Ca^{2+} measurements

Cells were seeded in 96-well plates, grown to ~70% confluency, and treated with serial concentrations of EpoTg or Tg for various time points. Subsequently, cells were washed once with Ca^{2+} Krebs solution (150 mM NaCl, 5.9 mM KCl, 1.2 mM $MgCl_2$, 11.6 mM HEPES (pH 7.3), 11.5 mM glucose and 1.5 mM $CaCl_2$) and loaded with 100 µl of 1.25 µM Fura-2 AM for 20 min. After another wash step, cells were incubated in Ca^{2+} Krebs solution for 30 min, before measurements on a FlexStation 3 microplate reader (Molecular Devices) by consecutive excitations at 340 and 380 nm, and measuring emitted fluorescence at 510 nm, every 5 s for 700 s. After the first 60 s, all wells were treated with 3 mM EGTA in Ca^{2+}-free Krebs for 60 s, before addition of 2 µM ATP, 1 µM Tg, or 2 µM ionomycin. Ca^{2+} release was plotted as ratio

of emitted Fura-2 fluorescence (F_{340}/F_{380}), and relative amounts of releasable Ca^{2+} was quantified by "area under the curve" calculations, using GraphPad Prism with a 10% threshold.

2.5 Direct ER Ca^{2+} measurements

Cells were transfected in 96-well plates with a plasmid expressing the Ca^{2+} indicator G-CEPIA1*er* (60 ng/well), kindly provided by Dr. M. Iino (University of Tokyo, Japan) [42] (Addgene plasmid #58215), using GenJet transfection reagent (Signagen, SL100489) according to the manufacturer's protocol. After 24 h of transfection, treatments were added, and the plate immediately placed in an IncuCyte ZOOM imaging system. G-CEPIA1*er* fluorescence was measured every hour from 3 image fields per well, thus registering the fluorescence from several thousand cells per treatment condition. To account for changes in fluorescence caused by alterations in G-CEPIA1*er* expression levels, integrated fluorescence intensity values were normalized to those obtained in DMSO control-treated cells at each time point. At 22 h, ER Ca^{2+} was purged with 5 μM A23187 to set the baseline level for quantifications.

2.6 Fluorescence microscopy of G-CEPIA1*er* and ER-Tracker Red

PC3 cells were seeded in 96-well plates for 2 d followed by 24 h transfection with the expression plasmid encoding G-CEPIA1*er*. Subsequently, the cell culture medium was replaced with Hank's Balanced Salt Solution (HBSS) containing 0.8 μM ER-Tracker Red (Thermo Fisher E34250). After 20 min incubation at 37°C in a humidified incubator with 5% CO_2, the staining solution was replaced with cell culture medium and immediately analysed with a Zeiss Axio Vert.A1 microscope using a 100x objective and appropriate filters to image the fluorescent signals from G-CEPIA1*er* (green) and ER-Tracker Red (red).

2.7 Autophagy assays

Bulk autophagy was assessed by measuring sequestration of lactate dehydrogenase (LDH) and degradation long-lived proteins, as described previously [43, 44].

2.8 Immunoblotting

Preparation of whole-cell lysates, SDS-PAGE, and immunoblot analysis were performed as described previously [3]. Primary antibodies were directed against: XBP1s (BioLegend; 647502, clone 143F), ATF4 (Cell Signaling Technology; CST#11815), GRP78/BiP (CST#3177), CHOP (CST#2895), Cleaved PARP (Asp214) (CST#5625), LC3B (CST#2775) and alpha-tubulin (Abcam, ab7291). Secondary horseradish peroxidase-conjugated goat anti-rabbit and rabbit anti-mouse antibodies were from Dako.

2.9 Statistical analyses

Significance was assumed at $P<0.05$, calculated with paired two-tailed t-test in GraphPad Prism.

3. Results

To assess cellular effects of gradual ER Ca^{2+} store depletion, we applied SERCA-inhibitory drugs at various concentrations. SERCA inhibition blocks the import of Ca^{2+} from the cytosol, resulting in ER Ca^{2+} depletion via various passive Ca^{2+}-leak mechanisms [45]. Thapsigargin (Tg) (Fig. 1A) is the most potent SERCA inhibitor and a frequently used experimental drug [46]. Additionally, various Tg analogues show promising potential in cancer-directed therapy [47]. Recently, we found that a sub-cytotoxic concentration of a Tg Epoxide analogue (EpoTg) (Fig. 1B) partially depleted ER Ca^{2+} after 24 h of treatment without concurrent UPR induction in PC3 [4], LNCaP and MCF7 cells (our unpublished observations). This suggested that cells may tolerate a partial, long-term ER Ca^{2+} depletion. However, we did not test dose-responses or kinetic effects. Here, we employ a series of concentrations and time points of EpoTg and Tg treatment to systematically examine the effects of ER Ca^{2+} depletion on UPR, autophagy, and cell death. We selected PC3 cells as our primary model, since they show a robust release of ER Ca^{2+} in response to Tg, and methodologically, Ca^{2+} assays are better applied to PC3 than LNCaP cells since PC3 cells adhere better to the tissue culture plate.

First, we established the dose-response and kinetic effects of EpoTg and Tg on cell death. PC3 cells were treated with a range of drug concentrations in the presence of the live/dead stain propidium iodide (PI), and real-time changes in cell confluency and cell death were monitored by live-cell phase-contrast and fluorescence imaging [4, 41]. Both EpoTg and Tg increased cell death in a dose- and time-dependent manner, with very similar kinetics (Fig. 2A and B). At concentrations above 500 nM for EpoTg, and above 5 nM for Tg, the ratio of PI-stained cells increased in a near-linear fashion over time, starting from around 15 h and increasing steadily up to 72 h (Fig. 2A and B). This was accompanied by a gradual decrease in cell confluency (the surface area covered by cells compared to the total surface area, as calculated from the recorded live-cell images by the IncuCyte software [41]) compared to control cells (Fig. 2C and D). Maximal cytotoxicity was obtained with 2500 nM for EpoTg (the highest concentration tested), and 30 nM for Tg (Fig. 2A and B; and see Fig. S1 for bar plot and statistical tests at the 60 h time point). As expected from earlier studies which have demonstrated that Tg activates apoptotic cell death [7-9, 36, 37, 48-50], EpoTg- and Tg-induced cell death was virtually completely abrogated by co-treatment with the caspase inhibitor Z-VAD-FMK, across all concentrations of EpoTg or Tg tested (Fig. 2E and F; Fig. S2A and B).

EpoTg showed barely detectable cytotoxicity at 300 nM, and was non-cytotoxic below that concentration (Fig. 2A; Fig. S1A). Interestingly, however, 150 - 300 nM EpoTg induced transient decreases in cell confluency compared to control cells (Fig. 2C), indicating cytostatic effects (a decrease in cell proliferation that is not caused by cell death). Almost identical results were obtained with 100-fold lower concentrations of Tg. Thus, Tg showed very minor cytotoxic effects at 3 nM, and was non-cytotoxic below that concentration (Fig. 2B; Fig. S1B). Moreover, Tg appeared to produce cytostatic effects in the 1.5 - 3 nM concentration window (Fig. 2B and D). In line with the notion that EpoTg and Tg produce cytostatic effects at these low concentrations, the decrease in cell confluency observed with 200 - 300 nM EpoTg or 2 - 3 nM Tg could not be rescued by co-treatment with Z-VAD-FMK, whereas the additional decrease in cell confluency observed with 2500 nM EpoTg or 30 nM Tg was reversed by Z-VAD-FMK

(Fig. 2G and H; Fig. S2C and D). In further support, cell viability assessment using the CellTiter 96 AQ_{ueous} One Solution assay produced very similar results; Z-VAD-FMK could not reverse the decrease in the number of viable cells observed with 200 - 300 nM EpoTg or 2 - 3 nM Tg, but did reverse the additional decrease observed with 2500 nM EpoTg or 30 nM Tg (Fig. S2 E and F). In conclusion, at concentrations between 150 - 300 nM (EpoTg) and 1.5 - 3 nM (Tg), EpoTg and Tg inhibit PC3 cell proliferation in a manner that is not caused by cell death. As the drug concentrations are gradually increased, the cytostatic effect is accompanied by the additional induction of apoptotic cell death, which increases strongly from 300 nM - 2500 nM EpoTg and from 3 nM - 30 nM Tg.

Next, we examined the effects of EpoTg and Tg on UPR. Activation of PERK leads to enhanced translation of ATF4, while activation of IRE1 leads to production of the alternatively spliced XBP1 (XBP1s), and all three arms of the UPR are involved in transcriptional upregulation of CHOP and BiP [2, 11, 51]. UPR activation is therefore reflected by increased protein levels of XBP1s, ATF4, CHOP and BiP. Moreover, the level of the autophagy-related phosphatidylethanolamine-conjugated LC3 protein (LC3-II) is known to be increased downstream of UPR signalling [52-55]. As shown in Fig. 3, cytotoxic concentrations of EpoTg (1500 nM) or Tg (30 nM) induced UPR in a strong and sustained manner. Increased levels of XBP1s, ATF4 and CHOP were observed after both 6 and 24 h of treatment (Fig. 3A-D), whereas BiP levels were slightly increased at 6 h and strongly increased at 24 h (Fig. 3A and E). Moreover, LC3-II levels were significantly elevated at 24 h (Fig. 3A and F). In agreement with the cytotoxicity data (Fig. 2A and B) and with an apoptotic mode of cell death (Fig. 2E and F; Fig S2A and B), these increases in XBP1s, ATF4, CHOP, BiP and LC3-II were accompanied by caspase-produced cleaved PARP (Fig. 3A and G). In contrast, treatment with 300 nM EpoTg or 3 nM Tg showed no or only very slight tendencies of effects on the levels of XBP1s, ATF4, CHOP, LC3-II, and cleaved PARP (Fig. 3; B-D and F-G), and only slightly enhanced BiP levels at 24 h (Fig. 3E). Importantly, non-cytotoxic concentrations of EpoTg (100 nM, 150 nM, or 200 nM) or Tg (1 nM, 1.5 nM, or 2 nM) did not induce any upregulation of XBP1s, ATF4, CHOP, BiP, LC3-II, or cleaved PARP, at any time point (Fig. 3). In conclusion, EpoTg/Tg-induced cell death correlates very well with the abilities of the drugs to induce UPR, whereas low drug concentrations produce cytostatic effects in the absence of UPR activation.

We subsequently asked whether non-cytotoxic concentrations of EpoTg or of Tg would have any short- or long-term effects on ER Ca^{2+} levels. To this end, we pre-treated PC3 cells with 100 - 200 nM EpoTg or with 1 - 2 nM Tg for various time points (1 h, 6 h, 24 h, 48 h, or 72 h), and assessed ER Ca^{2+} levels by measuring the amount of Ca^{2+} that could be released to the cytosol upon acute challenge with ATP. ATP binds to purinergic receptors, leading to rapid production of IP3 and to ensuing IP3R-mediated ER Ca^{2+} release [56]. Fig. 4A and B show the Ca^{2+} release curves obtained by ratiometric Fura-2 measurements of ATP-challenged cells pre-treated for 24 h with EpoTg (100 nM, 150 nM, or 200 nM) or Tg (1 nM, 1.5 nM, or 2 nM). Remarkably, we observed that treatment with these non-cytotoxic drug concentrations resulted in a strong and dose-dependent depletion of releasable ER Ca^{2+}, and after treatment with 200 nM EpoTg or 2 nM Tg for 24 h, the ability of ATP to increase cytosolic Ca^{2+} was almost completely abolished (Fig. 4A and B). Very similar results were obtained when a high

concentration of Tg (1 μM) was used instead of ATP to purge ER Ca^{2+} (Fig. S3A and B). To quantify effects of EpoTg and Tg on releasable ER Ca^{2+}, we calculated the area under the curve (AUC) for each condition and plotted it relative to DMSO control for each time point. This revealed that non-cytotoxic concentrations of EpoTg and Tg induce a time- and dose-dependent depletion of releasable ER Ca^{2+} (Fig. 4C and D; Fig S3C and D). In general, some depletion was noted after 1 h of treatment, whereas maximal effects were reached within 6 h, the exception being with the lowest concentration of EpoTg (100 nM), where maximal effects were observed at 48 - 72 h. With 200 nM EpoTg or 2 nM Tg, the depletion of releasable ER Ca^{2+} was complete or near-complete within 6 h. The depletion of ER Ca^{2+} was generally sustained, the exception being with the lowest concentration of Tg (1 nM), where the depleting effect gradually diminished between 6 and 72 h. Treatment with 200 nM or 2 nM Tg caused a complete or near-complete depletion of releasable ER Ca^{2+} throughout the period from 6 to 72 h (Fig. 4C and D; Fig. S3C and D). In further support, the Ca^{2+} ionophore ionomycin was also virtually unable to release Ca^{2+} in cells that had been pre-treated with 200 nM EpoTg for 6 h or more (Fig. S4).

These results were highly surprising, considering that the same concentrations of EpoTg (200 nM) and Tg (2 nM) neither induced UPR (Fig. 3) nor cell death (Fig. 2; Fig. S1). We therefore decided to assess the drug effects on ER Ca^{2+} in even further detail, and with a more direct method to measure ER Ca^{2+} levels. To that end, we transfected PC3 cells with the genetically encoded ER lumen-targeted fluorescent Ca^{2+} probe G-CEPIA1*er*, a GCaMP2-derivative optimized in terms of affinity and dynamic range for intraluminal ER Ca^{2+} imaging [42]. As expected, and as also confirmed previously in other cell lines [42], G-CEPIA1*er* localized to the ER in transfected PC3 cells (Fig. S5). Measurements of alterations in G-CEPIA1*er* fluorescence have so far been done by manual fluorescence microscopy, which only allows analysis of a rather limited amount of cells and is sensitive to subjective decisions with regard to the selection of transfected cells. To assess effects on ER Ca^{2+} levels in a larger sample of cells and in an unbiased manner, we monitored G-CEPIA1*er* fluorescence by automated live-cell fluorescence microscopy, with hourly measurements throughout 22 h of drug treatment. Overall, the results obtained with this method were in very good agreement with those obtained by the Fura-2-based quantifications of Ca^{2+} release described above. Thus, EpoTg and Tg reduced G-CEPIA1*er* fluorescence in a time- and concentration-dependent manner, and maximal or near-maximal effects were obtained within 6 h (Fig. 5A and B). Interestingly, however, the use of this more direct and sensitive method to measure ER Ca^{2+} levels enabled us to visualize tendencies of differences between non-UPR-inducing, non-cytotoxic drug concentrations versus UPR-inducing, cytotoxic concentrations. ER Ca^{2+} depletion was faster with high concentrations (near-complete effect within 2 h with > 500 nM EpoTg or > 10 nM Tg), and there was a tendency of stronger depletion. However, after a few hours of treatment with 300 nM EpoTg or 3 nM Tg, which have minimal effects on UPR and cell death, the decrease in G-CEPIA1*er* fluorescence approached that observed with the highest drug concentrations (Fig. 5A and B, and quantified for the 22 h time point in Fig. 5C and D). Taken together, our results demonstrate that total ER Ca^{2+} levels are strongly reduced by concentrations of EpoTg/Tg that have no or minimal effects on UPR and cell death. The gradual increase in UPR induction and cell death observed upon further increasing the drug

concentrations is accompanied by no or minimal changes in total ER Ca^{2+} levels, in terms of what can be measured by the Fura-2 and G-CEPIA1*er* methods (Fig. S6).

To examine whether this phenomenon was exclusive to PC3 cells, an androgen-resistant cell line, or whether it could be observed also in a different cell line, we next examined the relationship between ER Ca^{2+} levels versus induction of cell death and UPR in LNCaP cells, which are androgen sensitive. Like in PC3 cells, we observed a gradual time- and dose-dependent decrease in ER Ca^{2+} levels in LNCaP cells treated with increasing concentrations of EpoTg or Tg, as determined by the G-CEPIA1*er* method (Fig. 6A-D). ER Ca^{2+} was depleted with very similar kinetics in LNCaP as in PC3 cells, but required ~10-fold higher drug concentrations. Thus, a near-complete depletion of ER Ca^{2+}, as can be measured by G-CEPIA1*er*, was reached within 6 h of treatment with 1500 - 3000 nM EpoTg or 15 - 30 nM Tg (Fig. 6A-D). In contrast, cell death was not induced by 1500 nM EpoTg or 15 nM Tg, and only slightly increased by 3000 nM EpoTg or 30 nM Tg after 60 h of treatment (Fig. 6E and F), whereas strong induction of cell death required much higher concentrations of EpoTg and Tg in LNCaP cells (Fig. 6E and F; and see [4]). Just as in PC3 cells, the pattern of UPR induction in EpoTg/Tg-treated LNCaP cells correlated strongly with the level of cell death-induction rather than with the reduction of ER Ca^{2+} levels. Thus, UPR induction, as determined by analysis of XBP1s, ATF4, CHOP, and BiP protein levels occurred in the range of 3000 - 10000 nM EpoTg and 30 - 180 nM Tg, with an overall stronger induction at 10000 nM EpoTg and 180 nM Tg than at 3000 nM EpoTg or 30 nM Tg (Fig. 6G). A similar pattern was observed for the upregulation of LC3-II levels. The very strong reduction in ER Ca^{2+} levels observed from 250 - 1500 nM EpoTg and 2.5 - 15 nM Tg (Fig. 6A-D), was neither accompanied by UPR induction (Fig. 6G) nor cell death (Fig. 6E and F). As in PC3 cells, we observed reduced LNCaP cell proliferation with non-cytotoxic concentrations of EpoTg (500 - 1500 nM) and Tg (5 - 15 nM) (Fig. S7A and B), indicating cytostatic effects at these concentrations. Cleaved PARP was strongly detectable only at 24 h with 10000 nM EpoTg or 180 nM Tg (Fig. 6G). As in PC3 cells, and as previously demonstrated in Tg-treated LNCaP cells [50], both EpoTg- and Tg-induced cell death were virtually completely abrogated by co-treatment with Z-VAD-FMK (Fig. S7C and D). In conclusion, the relationship between the degree of ER Ca^{2+} depletion versus induction of cytostatic effects, UPR and cell death is very similar in PC3 and LNCaP cells.

Next, we asked whether the observed phenomena described above were solely related to ER Ca^{2+} depletion *per se*, or to a combination of potential nonspecific drug effects and ER Ca^{2+} depletion. To answer this question, we incubated PC3 cells with increasing concentrations of the Ca^{2+}-chelator EGTA in Ca^{2+}-free medium containing 10% FBS, to see if we could gradually drain out ER Ca^{2+} without the use of drugs. Indeed, measurements with G-CEPIA1*er* demonstrated a gradual decrease in ER Ca^{2+} levels as the EGTA concentration in the extracellular medium was increased (Fig. 7A and B). The levels of ER Ca^{2+} gradually and steeply declined at EGTA-concentrations above 0.40 mM, and plateaued at 0.48 mM, at the basal level observed after a purge of ER Ca^{2+} with the Ca^{2+} ionophore A23187 (Fig. 7B). Thus, addition of EGTA to the extracellular medium led to a very efficient and controlled depletion of ER Ca^{2+}. The kinetics of EGTA-induced ER Ca^{2+} depletion were initially slower than those observed with high concentrations of EpoTg or Tg, but maximal effects were reached within 4

h (Fig. 7A). By analysing the protein levels of XBP1s, ATF4, CHOP, and BiP at 8 h, we found that UPR activation required higher EGTA concentrations than those needed to reduce ER Ca^{2+} to the detection level of the G-CEPIA1*er* probe. Thus, although ER Ca^{2+} had reached the basal plateau level within 0.48 mM EGTA (Fig. 7A and B), concomitant increases in ATF4, CHOP, and BiP protein levels required 0.50 mM EGTA (Fig. 7C), and increased XBP1s levels were only observed above 0.50 mM EGTA (Fig. 7C). EGTA induced a more rapid cell death than that observed with EpoTg and Tg, and EGTA-induced cell death was only partially sensitive to Z-VAD-FMK (data not shown). This difference is likely due to the fact that high extracellular EGTA drains all Ca^{2+}-rich intracellular compartments, whereas EpoTg and Tg specifically inhibit the SERCA pump. Figure 7D shows the levels of cell death measured after 22 h of treatment in EGTA-containing medium. Some cell death was observed at EGTA-concentrations between 0.44 mM and 0.50 mM. However, when increasing the EGTA concentration from 0.50 mM to 0.80 mM, cell death was very strongly elevated (Fig. 7D), as was the UPR (Fig. 7C). This increase in cell death and UPR was not accompanied by any further decrease in ER Ca^{2+} levels as can be detected by the G-CEPIA1*er* probe (Fig. 7A and B). Taken together, these results confirm those obtained with the SERCA-inhibitory drugs, and thus indicate that the relationship between EpoTg/Tg-induced ER Ca^{2+} depletion versus induction of UPR and cell death are specifically due to the drug effects on ER Ca^{2+} levels rather than to a combined effect of ER Ca^{2+} depletion and putative nonspecific drug actions.

Tg inhibits bulk autophagy in a manner that is directly related to its calcium-modulating effect and does not involve UPR or bulk changes in cytosolic Ca^{2+} levels [3]. However, the relationship between the extent and duration of Tg-induced ER Ca^{2+} depletion versus autophagic activity is not known. As shown in Fig. 3A and F, LC3-II levels were strongly increased exclusively by high concentrations of Tg (30 nM) in PC3 cells, whereas LC3-II was not elevated by the lower Tg concentrations (1 - 3 nM), which were still efficient in depleting ER Ca^{2+} (Fig. 4 and 5). This might indicate that the effect of Tg on autophagy (like on UPR and cell death) requires an extremely efficient ER Ca^{2+} depletion. However, measurements of LC3-II levels cannot be used by themselves to reach conclusions about autophagy [57], and the increase observed with Tg may well be caused by transcriptional upregulation of LC3 [3]. We therefore employed additional methods to assess autophagic activity. Autophagy is characterised by the sequestration of cytoplasmic cargo, including long-lived proteins, into double-membrane structures termed autophagosomes, which fuse with lysosomes for degradation of the sequestered material. Tg inhibits bulk autophagy at the step of autophagosome formation, and thus reduces sequestration and degradation of cytoplasm, reflected by decreased sequestration of the cytosolic enzyme lactate dehydrogenase (LDH) and reduced degradation of long-lived proteins [3]. To assess the association between Tg-mediated autophagy inhibition and ER Ca^{2+} depletion, we pre-treated PC3 cells with increasing concentrations of Tg for 4 or 28 h, followed by amino acid starvation for 3 h to induce autophagy. Strikingly, starvation-induced bulk autophagic sequestration was significantly inhibited by 10 - 100 nM Tg, but not by 2 nM Tg (Fig. 8). In support, pre-treatment with 10 - 30 nM Tg, but not 1 - 3 nM Tg, reduced starvation-induced degradation of long-lived proteins (Fig. S8). Thus, the extensive and sustained reduction in total ER Ca^{2+} levels produced by 2-3 nM Tg (Fig. 4 and 5) does not restrict bulk autophagy.

4. Discussion

This study is the first to systematically explore the association between the extent and duration of ER Ca^{2+} depletion versus effects on UPR, cell death and autophagy. A graphical depiction of the major findings of the current study is shown in Fig. 9. Astoundingly, we find that cells can tolerate strong and sustained reduction in ER Ca^{2+} levels for 66 h (between 6 and 72 h of treatment with 200 nM EpoTg or 2 nM Tg in PC3 cells), without showing any signs of UPR, cell death, or inhibition of bulk autophagy. Notably, however, such conditions reduced cell proliferation. Much higher drug concentrations (e.g. 1500 nM EpoTg or 30 nM Tg in PC3 cells) were required for strong UPR induction (measured at 6 and 24 h), autophagy inhibition (measured at 4 to 28 h), and cell death (measured up to 72 h). Although there was a tendency of stronger ER Ca^{2+} depletion under the latter conditions, drug concentrations that induced minute amounts of UPR and cell death (300 nM EpoTg or 3 nM Tg in PC3 cells) showed an apparent similar extent of ER Ca^{2+} depletion as highly UPR-inducing, cytotoxic concentrations.

First of all we must consider whether the observed effects could be caused by nonspecific drug actions. We consider this highly unlikely, for several reasons. Firstly, Tg is an exceptionally potent and specific SERCA-inhibitor at low nanomolar concentrations, and nonspecific effects have only been reported in the micromolar range [58]. Secondly, EpoTg, which has lower affinity and a different mode of interaction with SERCA than Tg [4], provoked virtually identical cellular effects as Tg when used at 100-fold higher concentrations. Since Tg and EpoTg are very similar in structure (the only difference being a 7β,11α-diol in Tg, which is converted into a C7-C11 β-oxirane ring in EpoTg; Fig. 1) they likely share putative non-specific effects. Thus, if the effects reported herein were due to nonspecific effects, Tg and EpoTg would have shown similar dose-response properties, rather than the ~100-fold difference that we observed. Third, we demonstrated a very similar relationship between ER Ca^{2+} depletion versus induction of UPR and cell death when we used extracellular EGTA instead of the SERCA-inhibitory drugs to drain ER Ca^{2+}. Fourth, other agents that deplete ER Ca^{2+} also induce UPR [3, 33, 34, 59], inhibit autophagy [3, 31], and induce cell death [3, 34, 35, 60]. Finally, mechanistic considerations supporting that depletion of ER Ca^{2+} leads to UPR exists, namely that Ca^{2+} depletion leads to accumulation of unfolded proteins because the activities of ER-resident chaperones and enzymes depend on Ca^{2+} [2, 18, 19, 22]. In conclusion, the effects observed herein with EpoTg and Tg are highly unlikely to be caused by nonspecific drug actions.

We therefore consider two main possible explanations for our observations. First, since currently established ER Ca^{2+} probes deliberately have been developed to exert low Ca^{2+} affinity properties that are sensitive to changes compared to normal ER Ca^{2+} levels, they cannot detect changes in the extreme low ranges. Therefore, one possibility is that the observed effects on UPR and cell death require an extreme general depletion of ER Ca^{2+} levels, i.e. to an extent that is beyond what can be measured by the G-CEPIA1*er* probe. A second possibility is that the effects are not caused by bulk reduction in ER Ca^{2+} levels, but instead by Ca^{2+} depletion in areas of the ER that have a higher resistance to Ca^{2+} drainage than the rest of the ER.

The question then becomes which of the two above-mentioned possibilities are more likely; i.e. do the observed effects require an extreme general depletion of ER Ca^{2+} or are they specifically caused by Ca^{2+} depletion in areas of the ER which have a high resistance to Ca^{2+}

drainage? If the first scenario is true, it would imply that the activities of ER-resident chaperones and enzymes is largely maintained even under strongly reduced luminal Ca^{2+} levels (e.g. as that observed with 200 - 300 nM EpoTg or 2 - 3 nM Tg in PC3 cells), and therefore the UPR is not induced under such conditions. Is this a likely possibility in relation to what is known about the Ca^{2+}-dependencies of ER-resident chaperones and enzymes? Most of the Ca^{2+}-binding sites of ER-resident chaperones and foldases have low Ca^{2+} affinity, with reported Kd values ranging from 0.6 to 4.7 mM [22]. Since G-CEPIA1*er* has a Kd value of 0.672 mM [42], the strong decrease in its fluorescence that we observed already with non-cytotoxic, non-UPR-inducing drug concentrations would expectedly be accompanied by a massive decrease in the binding of Ca^{2+} to ER-resident chaperones and foldases. If they are still able to maintain their function during such conditions, it would mean that their activities are independent of low-affinity Ca^{2+} binding. Whether this may be, is yet to be fully determined. Calreticulin likely loses its chaperone function upon loss of low-affinity-bound Ca^{2+} [61, 62], and the foldase protein disulfide isomerase has been reported to only contain low-affinity (Kd 4.7 mM) Ca^{2+}-binding sites [63]. Moreover, the enzymatic activity of ER-UDPase is strongly decreased at levels below 0.5 mM Ca^{2+} [64], which may stall the calnexin cycle of protein folding [2]. From this it would appear unlikely that proper protein folding can be maintained under the conditions of strong ER Ca^{2+} reduction that we for instance observed with 200 - 300 nM EpoTg or 2 - 3 nM Tg in PC3 cells. However, the exact relationship between Ca^{2+} concentrations and the activities of most ER-resident chaperones and enzymes is still unknown, and thus it remains a possibility that it is the high-affinity Ca^{2+}-binding sites of such proteins that are most critical in relation to protein folding *in vivo*, whereas low-affinity sites may mainly act to buffer Ca^{2+} and thus secure the basis for Ca^{2+}-inducing signalling.

Alternatively, in line with the second scenario, it may be that protein folding predominantly occurs in areas of the ER that are more shielded from fluctuations in Ca^{2+} levels than other parts of the ER [65, 66]. Such areas may exist due to heterogeneous distribution of ER Ca^{2+}-handling proteins, i.e. Ca^{2+}-binding proteins, Ca^{2+} pumps and Ca^{2+} channels [65-67]. According to our results and the second scenario, a putative "protein folding area" would be characterized by higher resistance to Ca^{2+} depletion by SERCA inhibitors or extracellular EGTA than the rest of the ER. As the SERCA-inhibitor or EGTA concentration is increased, the bulk of ER Ca^{2+}, presumably that residing in so called "Ca^{2+} homeostasis and signaling areas" [66], will be depleted first, but not give rise to UPR, since the "protein folding area" still maintains high enough Ca^{2+} concentrations for its activities. This would be the situation in PC3 cells treated with concentrations up to 300 nM EpoTg, 3 nM Tg, or 0.48 mM EGTA. Upon further increase in SERCA-inhibitor or EGTA concentrations, the Ca^{2+} concentration in the "protein folding area" is gradually reduced to levels incompatible with protein folding, and thus the UPR and, eventually, cell death is induced. Although the ER normally appears to be one, continuously connected Ca^{2+} pool (i.e. not containing physically separated compartments) [68, 69], heterogeneous distribution of ER Ca^{2+} has been reported in many different cell types under various conditions [66, 67, 70-72]. Moreover, the Ca^{2+} ionophore ionomycin may induce ER fragmentation [68, 73]. Tg was described to promote ER fragmentation in mouse fibroblasts [68], but not in HEK293 cells [74]. In line with the latter, we did not observe fragmentation of the G-CEPIA1*er* signal in Tg-treated PC3 and LNCaP cells (data not shown). Intriguingly,

however, our preliminary examinations suggest that non-UPR-inducing EpoTg/Tg concentrations preferentially deplete peripheral ER Ca^{2+}, thus leaving G-CEPIA1*er* fluorescence predominantly in a narrow perinuclear region, whereas the reduction appears more even in cells treated with UPR-inducing drug concentrations (data not shown). This would indicate that a perinuclear area of the ER may represent a "protein folding area" that is more resistant to Ca^{2+} depletion and thus has a higher threshold for SERCA inhibition-induced UPR and cell death. This remains an attractive hypothesis for now, as addressing it further will require a very careful and detailed study of the exact intra-lumenal distributions of ER Ca^{2+}, Ca^{2+}-handling proteins, and protein folding activities, which is beyond the scope of the current study. Importantly, we believe that the conditions identified in the current study where the overall levels of ER Ca^{2+} are strongly reduced but where there is no induction of UPR or cell death, will be very useful experimental tools to further pursue the above-mentioned questions and hypotheses.

Also in relation to the observed effects on bulk autophagy, both types of scenarios described above are possible; either autophagy inhibition requires an extreme overall depletion of ER Ca^{2+}, or Ca^{2+} depletion of ER domains that are more resistant to Ca^{2+} drainage than the rest of the ER. It is intriguing that inhibition of bulk autophagy occurs with the same Tg concentration-dependency as induction of UPR and cell death, even though Tg-mediated UPR-induction is not required for its ability to block autophagy [3]. Thus, the mediating mechanisms may be linked, yet different. One possibility is that the autophagic process depends on the correct folding of proteins in the ER, and thus bulk autophagy is blocked if the ER protein folding activity is severely impaired. Another interesting possibility is that ER Ca^{2+} depletion may block autophagy via regulation of another calcium store. ER shows considerable crosstalk and exchange of Ca^{2+} with mitochondria [75] and lysosomes [76-79], and Ca^{2+} signalling from both these compartments is implicated in autophagy regulation [80, 81]. Cell death induction has under certain circumstances been attributed to mitochondrial Ca^{2+} overload [82, 83], however when using the mitochondrially targeted CEPIA-3mt Ca^{2+} probe we did not observe any indication of mitochondrial Ca^{2+} overload in EpoTg- or Tg-treated PC3 cells (data not shown).

Interestingly, the gradual decrease in total ER Ca^{2+} levels observed between 100 - 300 nM EpoTg and 1 - 3 nM Tg correlated with a decrease in PC3 cell confluence, which could not be accounted for by cell death. This indicates that high ER Ca^{2+} levels are required for optimal cell growth, and that even partial depletion of total ER Ca^{2+} levels is sufficient to produce cytostatic effects. The effect appears to be unrelated to alterations in bulk autophagy, and since no, or hardly any UPR was induced at these drug concentrations, it is likely mediated by non-UPR mechanisms. At higher concentrations of EpoTg (> 300 nM) or Tg (> 3 nM), we observed a gradual, caspase-dependent increase in cell death, which is highly likely to be caused by UPR [4-9]. Some studies have indicated that increases in cytosolic Ca^{2+} levels, mediated via store-operated Ca^{2+} entry (SOCE), are required for ER Ca^{2+}-depletion-induced cell death [84, 85]. However, we have previously shown that depletion of two key SOCE components, Orai1 and STIM1, does not reduce Tg cytotoxicity in PC3, LNCaP or MCF7 cells [4]. Moreover, we have found that Tg and various Tg analogues produce maximal cell death at concentrations that are

substantially lower than those needed to induce detectable increases in cytosolic Ca^{2+} levels [3, 4]. Thus, SOCE-mediated increase in cytosolic Ca^{2+} does not seem to be obligatory for ER Ca^{2+}-depletion-induced cell death. Combined with the results from our current study, it appears that ER Ca^{2+}-depletion-induced activation of SOCE to increase bulk cytosolic Ca^{2+} levels requires an even more extreme depletion of ER Ca^{2+} levels than that needed to inhibit bulk autophagy or activate UPR-induced cell death.

Our observations are of considerable interest with respect to the implication of decreased expression or function of SERCA, and lowered ER Ca^{2+} levels in various diseases [23-30, 86, 87], and SERCA-targeting medical drugs [47]. Although our results imply that a strong reduction of steady-state ER Ca^{2+} does not necessarily affect UPR, autophagy, or cell death, it does produce cytostatic effects, and importantly, it remains entirely possible that disease-affected tissues or cells with lowered ER Ca^{2+} levels have an increased susceptibility to environmental and/or therapeutic cues that provoke ER Ca^{2+} release. Under such conditions it may well be that UPR and other effects are induced, thereby explaining the association between such disease states and elevated UPR levels [23]. EpoTg and Tg interact differently with SERCA, and unlike Tg, which completely blocks SERCA activity *in vitro*, EpoTg maximally reduces SERCA activity by 90% [4]. It is therefore very interesting to note that we could equally well observe cytostatic effects, UPR induction and Z-VAD-FMK-sensitive cell death with EpoTg as with Tg. Hence, all these effects can be achieved without complete inhibition of SERCA. In conclusion, the results presented here shed important new light on the link between ER Ca^{2+} depletion and cellular outcomes with relevance to disease states characterized by defects in SERCA and ER Ca^{2+} homeostasis.

Conflict of interests

The authors declare no conflict of interest with the contents of this article.

Acknowledgments

We thank Mart Bittremieux (KU Leuven, Belgium) for help with setting up Ca^{2+} assays. This work was generously supported by grants (to NE) from the Research Council of Norway and the University of Oslo (grant number 230686), the Nansen Foundation, and the Anders Jahre Foundation. PS is supported by a grant from The Lundbeck Foundation (to PN and NE; grant number R191-2015-1512). JBP was supported by grants G063413N and G092715N of the Fund for Scientific Research - Flanders.

References

[1] J. Krebs, L.B. Agellon, M. Michalak, Ca(2+) homeostasis and endoplasmic reticulum (ER) stress: An integrated view of calcium signaling, Biochemical and biophysical research communications, 460 (2015) 114-121.

[2] M. Schroder, Endoplasmic reticulum stress responses, Cellular and molecular life sciences : CMLS, 65 (2008) 862-894.

[3] N. Engedal, M.L. Torgersen, I.J. Guldvik, S.J. Barfeld, D. Bakula, F. Saetre, L.K. Hagen, J.B. Patterson, T. Proikas-Cezanne, P.O. Seglen, A. Simonsen, I.G. Mills, Modulation of intracellular calcium homeostasis blocks autophagosome formation, Autophagy, 9 (2013) 1475-1490.

[4] P. Sehgal, P. Szalai, C. Olesen, H.A. Praetorius, P. Nissen, S.B. Christensen, N. Engedal, J.V. Moller, Inhibition of the sarco/endoplasmic reticulum (ER) Ca(2+)-ATPase by thapsigargin analogs induces cell death via ER Ca(2+) depletion and the unfolded protein response, The Journal of biological chemistry, 292 (2017) 19656-19673.

[5] R. Sano, J.C. Reed, ER stress-induced cell death mechanisms, Biochimica et biophysica acta, 1833 (2013) 3460-3470.

[6] N. Sovolyova, S. Healy, A. Samali, S.E. Logue, Stressed to death - mechanisms of ER stress-induced cell death, Biological chemistry, 395 (2014) 1-13.

[7] H. Yamaguchi, H.G. Wang, CHOP is involved in endoplasmic reticulum stress-induced apoptosis by enhancing DR5 expression in human carcinoma cells, The Journal of biological chemistry, 279 (2004) 45495-45502.

[8] C. Humeres, J. Montenegro, M. Varela, P. Ayala, R. Vivar, A. Letelier, I. Olmedo, M. Catalan, C. Rivas, P. Baeza, C. Munoz, L. Garcia, S. Lavandero, G. Diaz-Araya, 4-Phenylbutyric acid prevent cytotoxicity induced by thapsigargin in rat cardiac fibroblast, Toxicology in vitro : an international journal published in association with BIBRA, 28 (2014) 1443-1448.

[9] M. Lu, D.A. Lawrence, S. Marsters, D. Acosta-Alvear, P. Kimmig, A.S. Mendez, A.W. Paton, J.C. Paton, P. Walter, A. Ashkenazi, Opposing unfolded-protein-response signals converge on death receptor 5 to control apoptosis, Science, 345 (2014) 98-101.

[10] C. Hetz, F.R. Papa, The Unfolded Protein Response and Cell Fate Control, Molecular cell, 69 (2018) 169-181.

[11] J.D. Malhotra, R.J. Kaufman, The endoplasmic reticulum and the unfolded protein response, Seminars in cell & developmental biology, 18 (2007) 716-731.

[12] S. Deegan, S. Saveljeva, A.M. Gorman, A. Samali, Stress-induced self-cannibalism: on the regulation of autophagy by endoplasmic reticulum stress, Cellular and molecular life sciences : CMLS, 70 (2013) 2425-2441.

[13] J.A. Morris, A.J. Dorner, C.A. Edwards, L.M. Hendershot, R.J. Kaufman, Immunoglobulin binding protein (BiP) function is required to protect cells from endoplasmic reticulum stress but is not

required for the secretion of selective proteins, The Journal of biological chemistry, 272 (1997) 4327-4334.

[14] A. Bertolotti, Y. Zhang, L.M. Hendershot, H.P. Harding, D. Ron, Dynamic interaction of BiP and ER stress transducers in the unfolded-protein response, Nature cell biology, 2 (2000) 326-332.

[15] M. Carrara, F. Prischi, P.R. Nowak, M.C. Kopp, M.M. Ali, Noncanonical binding of BiP ATPase domain to Ire1 and Perk is dissociated by unfolded protein CH1 to initiate ER stress signaling, eLife, 4 (2015).

[16] N. Amin-Wetzel, R.A. Saunders, M.J. Kamphuis, C. Rato, S. Preissler, H.P. Harding, D. Ron, A J-Protein Co-chaperone Recruits BiP to Monomerize IRE1 and Repress the Unfolded Protein Response, Cell, 171 (2017) 1625-1637 e1613.

[17] M.C. Kopp, P.R. Nowak, N. Larburu, C.J. Adams, M.M. Ali, In vitro FRET analysis of IRE1 and BiP association and dissociation upon endoplasmic reticulum stress, eLife, 7 (2018).

[18] H.F. Lodish, N. Kong, Perturbation of cellular calcium blocks exit of secretory proteins from the rough endoplasmic reticulum, The Journal of biological chemistry, 265 (1990) 10893-10899.

[19] H.F. Lodish, N. Kong, L. Wikstrom, Calcium is required for folding of newly made subunits of the asialoglycoprotein receptor within the endoplasmic reticulum, The Journal of biological chemistry, 267 (1992) 12753-12760.

[20] C. Booth, G.L. Koch, Perturbation of cellular calcium induces secretion of luminal ER proteins, Cell, 59 (1989) 729-737.

[21] C.K. Suzuki, J.S. Bonifacino, A.Y. Lin, M.M. Davis, R.D. Klausner, Regulating the retention of T-cell receptor alpha chain variants within the endoplasmic reticulum: Ca(2+)-dependent association with BiP, The Journal of cell biology, 114 (1991) 189-205.

[22] H. Coe, M. Michalak, Calcium binding chaperones of the endoplasmic reticulum, General physiology and biophysics, 28 Spec No Focus (2009) F96-F103.

[23] D. Mekahli, G. Bultynck, J.B. Parys, H. De Smedt, L. Missiaen, Endoplasmic-reticulum calcium depletion and disease, Cold Spring Harbor perspectives in biology, 3 (2011) 10.1101/cshperspect.a004317.

[24] M. Bittremieux, J.B. Parys, P. Pinton, G. Bultynck, ER functions of oncogenes and tumor suppressors: Modulators of intracellular Ca(2+) signaling, Biochimica et biophysica acta, 1863 (2016) 1364-1378.

[25] K.M. Doyle, D. Kennedy, A.M. Gorman, S. Gupta, S.J. Healy, A. Samali, Unfolded proteins and endoplasmic reticulum stress in neurodegenerative disorders, Journal of cellular and molecular medicine, 15 (2011) 2025-2039.

[26] A. Guerrero-Hernandez, A. Verkhratsky, Calcium signalling in diabetes, Cell calcium, 56 (2014) 297-301.

[27] A. Kushnir, B. Wajsberg, A.R. Marks, Ryanodine receptor dysfunction in human disorders, Biochimica et biophysica acta, (2018) 10.1016/j.bbamcr.2018.1007.1011.

[28] L. Ozcan, I. Tabas, Calcium signalling and ER stress in insulin resistance and atherosclerosis, Journal of internal medicine, 280 (2016) 457-464.

[29] V. Tadic, T. Prell, J. Lautenschlaeger, J. Grosskreutz, The ER mitochondria calcium cycle and ER stress response as therapeutic targets in amyotrophic lateral sclerosis, Frontiers in cellular neuroscience, 8 (2014) 147.

[30] W.A. Wang, J. Groenendyk, M. Michalak, Endoplasmic reticulum stress associated responses in cancer, Biochimica et biophysica acta, 1843 (2014) 2143-2149.

[31] P.B. Gordon, I. Holen, M. Fosse, J.S. Rotnes, P.O. Seglen, Dependence of hepatocytic autophagy on intracellularly sequestered calcium, The Journal of biological chemistry, 268 (1993) 26107-26112.

[32] H.P. Harding, Y. Zhang, H. Zeng, I. Novoa, P.D. Lu, M. Calfon, N. Sadri, C. Yun, B. Popko, R. Paules, D.F. Stojdl, J.C. Bell, T. Hettmann, J.M. Leiden, D. Ron, An integrated stress response regulates amino acid metabolism and resistance to oxidative stress, Molecular cell, 11 (2003) 619-633.

[33] E. Kyriakakis, M. Philippova, M.B. Joshi, D. Pfaff, V. Bochkov, T. Afonyushkin, P. Erne, T.J. Resink, T-cadherin attenuates the PERK branch of the unfolded protein response and protects vascular endothelial cells from endoplasmic reticulum stress-induced apoptosis, Cellular signalling, 22 (2010) 1308-1316.

[34] S. Nozaki, G.W. Sledge, Jr., H. Nakshatri, Repression of GADD153/CHOP by NF-kappaB: a possible cellular defense against endoplasmic reticulum stress-induced cell death, Oncogene, 20 (2001) 2178-2185.

[35] C.W. Shu, F.C. Sun, J.H. Cho, C.C. Lin, P.F. Liu, P.Y. Chen, M.D. Chang, H.W. Fu, Y.K. Lai, GRP78 and Raf-1 cooperatively confer resistance to endoplasmic reticulum stress-induced apoptosis, Journal of cellular physiology, 215 (2008) 627-635.

[36] R. Skryma, P. Mariot, X.L. Bourhis, F.V. Coppenolle, Y. Shuba, F. Vanden Abeele, G. Legrand, S. Humez, B. Boilly, N. Prevarskaya, Store depletion and store-operated Ca2+ current in human prostate cancer LNCaP cells: involvement in apoptosis, The Journal of physiology, 527 Pt 1 (2000) 71-83.

[37] I.E. Wertz, V.M. Dixit, Characterization of calcium release-activated apoptosis of LNCaP prostate cancer cells, The Journal of biological chemistry, 275 (2000) 11470-11477.

[38] A. Williams, S. Sarkar, P. Cuddon, E.K. Ttofi, S. Saiki, F.H. Siddiqi, L. Jahreiss, A. Fleming, D. Pask, P. Goldsmith, C.J. O'Kane, R.A. Floto, D.C. Rubinsztein, Novel targets for Huntington's disease in an mTOR-independent autophagy pathway, Nature chemical biology, 4 (2008) 295-305.

[39] I. Yoshida, A. Monji, K. Tashiro, K. Nakamura, R. Inoue, S. Kanba, Depletion of intracellular Ca2+ store itself may be a major factor in thapsigargin-induced ER stress and apoptosis in PC12 cells, Neurochemistry international, 48 (2006) 696-702.

[40] C.M. Jakobsen, S.R. Denmeade, J.T. Isaacs, A. Gady, C.E. Olsen, S.B. Christensen, Design, synthesis, and pharmacological evaluation of thapsigargin analogues for targeting apoptosis to prostatic cancer cells, Journal of medicinal chemistry, 44 (2001) 4696-4703.

[41] P. Szalai, N. Engedal, An Image-based Assay for High-throughput Analysis of Cell Proliferation and Cell Death of Adherent Cells, Bio-Protocol, 8 (2018) 10.21769/BioProtoc.22835.

[42] J. Suzuki, K. Kanemaru, K. Ishii, M. Ohkura, Y. Okubo, M. Iino, Imaging intraorganellar Ca2+ at subcellular resolution using CEPIA, Nature communications, 5 (2014) 4153.

[43] M. Luhr, P. Szalai, N. Engedal, The Lactate Dehydrogenase Sequestration Assay - A Simple and Reliable Method to Determine Bulk Autophagic Sequestration Activity in Mammalian Cells, J Vis Exp, 137 (2018) 10.3791/57971.

[44] M. Luhr, F. Sætre, N. Engedal, The Long-lived Protein Degradation Assay: an Efficient Method for Quantitative Determination of the Autophagic Flux of Endogenous Proteins in Adherent Cell Lines, Bio-Protocol, 8 (2018) e2836.

[45] C. Camello, R. Lomax, O.H. Petersen, A.V. Tepikin, Calcium leak from intracellular stores--the enigma of calcium signalling, Cell calcium, 32 (2002) 355-361.

[46] F. Michelangeli, J.M. East, A diversity of SERCA Ca2+ pump inhibitors, Biochemical Society transactions, 39 (2011) 789-797.

[47] N.T. Doan, E.S. Paulsen, P. Sehgal, J.V. Moller, P. Nissen, S.R. Denmeade, J.T. Isaacs, C.A. Dionne, S.B. Christensen, Targeting thapsigargin towards tumors, Steroids, 97 (2015) 2-7.

[48] Y. Kaneko, A. Tsukamoto, Thapsigargin-induced persistent intracellular calcium pool depletion and apoptosis in human hepatoma cells, Cancer letters, 79 (1994) 147-155.

[49] X.M. Qi, H. He, H. Zhong, C.W. Distelhorst, Baculovirus p35 and Z-VAD-fmk inhibit thapsigargin-induced apoptosis of breast cancer cells, Oncogene, 15 (1997) 1207-1212.

[50] N. Engedal, C.G. Korkmaz, F. Saatcioglu, C-Jun N-terminal kinase is required for phorbol ester- and thapsigargin-induced apoptosis in the androgen responsive prostate cancer cell line LNCaP, Oncogene, 21 (2002) 1017-1027.

[51] S. Takayanagi, R. Fukuda, Y. Takeuchi, S. Tsukada, K. Yoshida, Gene regulatory network of unfolded protein response genes in endoplasmic reticulum stress, Cell stress & chaperones, 18 (2013) 11-23.

[52] M. Ogata, S. Hino, A. Saito, K. Morikawa, S. Kondo, S. Kanemoto, T. Murakami, M. Taniguchi, I. Tanii, K. Yoshinaga, S. Shiosaka, J.A. Hammarback, F. Urano, K. Imaizumi, Autophagy is activated for cell survival after endoplasmic reticulum stress, Molecular and cellular biology, 26 (2006) 9220-9231.

[53] Y. Kouroku, E. Fujita, I. Tanida, T. Ueno, A. Isoai, H. Kumagai, S. Ogawa, R.J. Kaufman, E. Kominami, T. Momoi, ER stress (PERK/eIF2alpha phosphorylation) mediates the polyglutamine-induced LC3 conversion, an essential step for autophagy formation, Cell death and differentiation, 14 (2007) 230-239.

[54] L.S. Hart, J.T. Cunningham, T. Datta, S. Dey, F. Tameire, S.L. Lehman, B. Qiu, H. Zhang, G. Cerniglia, M. Bi, Y. Li, Y. Gao, H. Liu, C. Li, A. Maity, A. Thomas-Tikhonenko, A.E. Perl, A. Koong, S.Y. Fuchs, J.A. Diehl, I.G. Mills, D. Ruggero, C. Koumenis, ER stress-mediated autophagy promotes Myc-dependent transformation and tumor growth, The Journal of clinical investigation, 122 (2012) 4621-4634.

[55] Y. Shimodaira, S. Takahashi, Y. Kinouchi, K. Endo, H. Shiga, Y. Kakuta, M. Kuroha, T. Shimosegawa, Modulation of endoplasmic reticulum (ER) stress-induced autophagy by C/EBP homologous protein (CHOP) and inositol-requiring enzyme 1alpha (IRE1alpha) in human colon cancer cells, Biochemical and biophysical research communications, 445 (2014) 524-533.

[56] L.H. Jiang, F. Mousawi, X. Yang, S. Roger, ATP-induced Ca(2+)-signalling mechanisms in the regulation of mesenchymal stem cell migration, Cellular and molecular life sciences : CMLS, 74 (2017) 3697-3710.

[57] D.J. Klionsky, K. Abdelmohsen, A. Abe, M.J. Abedin, H. Abeliovich, A. Acevedo Arozena, H. Adachi, C.M. Adams, P.D. Adams, K. Adeli, P.J. Adhihetty, S.G. Adler, G. Agam, R. Agarwal, M.K. Aghi, M. Agnello, P. Agostinis, P.V. Aguilar, J. Aguirre-Ghiso, E.M. Airoldi, S. Ait-Si-Ali, T. Akematsu, E.T. Akporiaye, M. Al-Rubeai, G.M. Albaiceta, C. Albanese, D. Albani, M.L. Albert, J. Aldudo, H. Algul, et al., Guidelines for the use and interpretation of assays for monitoring autophagy (3rd edition), Autophagy, 12 (2016) 1-222.

[58] A. Toth, N. Kedei, T. Szabo, Y. Wang, P.M. Blumberg, Thapsigargin binds to and inhibits the cloned vanilloid receptor-1, Biochemical and biophysical research communications, 293 (2002) 777-782.

[59] J. Zhou, B. Mao, Q. Zhou, D. Ding, M. Wang, P. Guo, Y. Gao, J.W. Shay, Z. Yuan, Y.S. Cong, Endoplasmic reticulum stress activates telomerase, Aging cell, 13 (2014) 197-200.

[60] B.J. Gwag, L.M. Canzoniero, S.L. Sensi, J.A. Demaro, J.Y. Koh, M.P. Goldberg, M. Jacquin, D.W. Choi, Calcium ionophores can induce either apoptosis or necrosis in cultured cortical neurons, Neuroscience, 90 (1999) 1339-1348.

[61] E.F. Corbett, K. Oikawa, P. Francois, D.C. Tessier, C. Kay, J.J. Bergeron, D.Y. Thomas, K.H. Krause, M. Michalak, Ca2+ regulation of interactions between endoplasmic reticulum chaperones, The Journal of biological chemistry, 274 (1999) 6203-6211.

[62] E.F. Corbett, K.M. Michalak, K. Oikawa, S. Johnson, I.D. Campbell, P. Eggleton, C. Kay, M. Michalak, The conformation of calreticulin is influenced by the endoplasmic reticulum luminal environment, The Journal of biological chemistry, 275 (2000) 27177-27185.

[63] D. Lebeche, H.A. Lucero, B. Kaminer, Calcium binding properties of rabbit liver protein disulfide isomerase, Biochemical and biophysical research communications, 202 (1994) 556-561.

[64] E.S. Trombetta, A. Helenius, Glycoprotein reglucosylation and nucleotide sugar utilization in the secretory pathway: identification of a nucleoside diphosphatase in the endoplasmic reticulum, The EMBO journal, 18 (1999) 3282-3292.

[65] E. Rooney, J. Meldolesi, The endoplasmic reticulum in PC12 cells. Evidence for a mosaic of domains differently specialized in Ca2+ handling, The Journal of biological chemistry, 271 (1996) 29304-29311.

[66] S. Papp, E. Dziak, M. Michalak, M. Opas, Is all of the endoplasmic reticulum created equal? The effects of the heterogeneous distribution of endoplasmic reticulum Ca2+-handling proteins, The Journal of cell biology, 160 (2003) 475-479.

[67] O. Baumann, B. Walz, Endoplasmic reticulum of animal cells and its organization into structural and functional domains, International review of cytology, 205 (2001) 149-214.

[68] K. Subramanian, T. Meyer, Calcium-induced restructuring of nuclear envelope and endoplasmic reticulum calcium stores, Cell, 89 (1997) 963-971.

[69] O.H. Petersen, A. Tepikin, M.K. Park, The endoplasmic reticulum: one continuous or several separate Ca(2+) stores?, Trends in neurosciences, 24 (2001) 271-276.

[70] V.A. Golovina, M.P. Blaustein, Spatially and functionally distinct Ca2+ stores in sarcoplasmic and endoplasmic reticulum, Science, 275 (1997) 1643-1648.

[71] M. Montero, J. Alvarez, W.J. Scheenen, R. Rizzuto, J. Meldolesi, T. Pozzan, Ca2+ homeostasis in the endoplasmic reticulum: coexistence of high and low [Ca2+] subcompartments in intact HeLa cells, The Journal of cell biology, 139 (1997) 601-611.

[72] M.P. Blaustein, V.A. Golovina, Structural complexity and functional diversity of endoplasmic reticulum Ca(2+) stores, Trends in neurosciences, 24 (2001) 602-608.

[73] M.K. Park, O.H. Petersen, A.V. Tepikin, The endoplasmic reticulum as one continuous Ca(2+) pool: visualization of rapid Ca(2+) movements and equilibration, The EMBO journal, 19 (2000) 5729-5739.

[74] C.M. Ribeiro, R.R. McKay, E. Hosoki, G.S. Bird, J.W. Putney, Jr., Effects of elevated cytoplasmic calcium and protein kinase C on endoplasmic reticulum structure and function in HEK293 cells, Cell calcium, 27 (2000) 175-185.

[75] S. Marchi, M. Bittremieux, S. Missiroli, C. Morganti, S. Patergnani, L. Sbano, A. Rimessi, M. Kerkhofs, J.B. Parys, G. Bultynck, C. Giorgi, P. Pinton, Endoplasmic Reticulum-Mitochondria Communication Through Ca(2+) Signaling: The Importance of Mitochondria-Associated Membranes (MAMs), Advances in experimental medicine and biology, 997 (2017) 49-67.

[76] B.S. Kilpatrick, E.R. Eden, A.H. Schapira, C.E. Futter, S. Patel, Direct mobilisation of lysosomal Ca2+ triggers complex Ca2+ signals, Journal of cell science, 126 (2013) 60-66.

[77] C.I. Lopez-Sanjurjo, S.C. Tovey, D.L. Prole, C.W. Taylor, Lysosomes shape Ins(1,4,5)P3-evoked Ca2+ signals by selectively sequestering Ca2+ released from the endoplasmic reticulum, Journal of cell science, 126 (2013) 289-300.

[78] A.J. Morgan, L.C. Davis, S.K. Wagner, A.M. Lewis, J. Parrington, G.C. Churchill, A. Galione, Bidirectional Ca(2)(+) signaling occurs between the endoplasmic reticulum and acidic organelles, The Journal of cell biology, 200 (2013) 789-805.

[79] A.G. Garrity, W. Wang, C.M. Collier, S.A. Levey, Q. Gao, H. Xu, The endoplasmic reticulum, not the pH gradient, drives calcium refilling of lysosomes, eLife, 5 (2016).

[80] S. Di Paola, A. Scotto-Rosato, D.L. Medina, TRPML1: The Ca((2+))retaker of the lysosome, Cell calcium, 69 (2018) 112-121.

[81] R.M. La Rovere, G. Roest, G. Bultynck, J.B. Parys, Intracellular Ca(2+) signaling and Ca(2+) microdomains in the control of cell survival, apoptosis and autophagy, Cell calcium, 60 (2016) 74-87.

[82] M. Crompton, The mitochondrial permeability transition pore and its role in cell death, The Biochemical journal, 341 (Pt 2) (1999) 233-249.

[83] B. Yun, H. Lee, M. Ghosh, B.F. Cravatt, K.L. Hsu, J.V. Bonventre, H. Ewing, M.H. Gelb, C.C. Leslie, Serine hydrolase inhibitors block necrotic cell death by preventing calcium overload of the mitochondria and permeability transition pore formation, The Journal of biological chemistry, 289 (2014) 1491-1504.

[84] M. Flourakis, V. Lehen'kyi, B. Beck, M. Raphael, M. Vandenberghe, F.V. Abeele, M. Roudbaraki, G. Lepage, B. Mauroy, C. Romanin, Y. Shuba, R. Skryma, N. Prevarskaya, Orai1 contributes to the establishment of an apoptosis-resistant phenotype in prostate cancer cells, Cell death & disease, 1 (2010) e75.

[85] B. Tombal, A.T. Weeraratna, S.R. Denmeade, J.T. Isaacs, Thapsigargin induces a calmodulin/calcineurin-dependent apoptotic cascade responsible for the death of prostatic cancer cells, The Prostate, 43 (2000) 303-317.

[86] L. Lipskaia, J.S. Hulot, A.M. Lompre, Role of sarco/endoplasmic reticulum calcium content and calcium ATPase activity in the control of cell growth and proliferation, Pflugers Archiv : European journal of physiology, 457 (2009) 673-685.

[87] E.R. Chemaly, L. Troncone, D. Lebeche, SERCA control of cell death and survival, Cell calcium, 69 (2018) 46-61.

Figure Legends

Fig. 1. Chemical structure of Tg (A) and EpoTg (B).

Fig. 2. EpoTg and Tg induce cell death and growth inhibition in a dose-dependent manner. A, B: PC3 cells were seeded in 96-well plates 2 d prior to treatment with the indicated concentrations of EpoTg (A), Tg (B), or DMSO control (0.05%), together with 2.5 µg/ml propidium iodide. Cell death was monitored by live-cell fluorescence imaging (IncuCyte ZOOM) every 3 h. Relative cell death is plotted over time as ratio of red fluorescent- to total cell confluence, normalized to the average ratio of each experiment. Mean±SEM of 3 independent experiments. C, D: Relative cell confluency (recorded by live-cell phase-contrast imaging in the same experiments as described in A and B), plotted over time and normalized to the confluency of each condition at 0 h. Mean±SEM of 3 independent experiments. E, F: PC3 cells were treated with the indicated concentrations of EpoTg (E) or Tg (F) in the absence or presence of 50 µM Z-VAD-FMK (zVAD), and cell death was measured as in A and B after 60 h of treatment. G, H: PC3 cells were treated with the indicated concentrations of EpoTg (E) or Tg (F) in the absence or presence of 50 µM Z-VAD-FMK (zVAD) or DMSO control (0.05%), and cell confluence was determined as in C and D after 44 h of treatment. For E-H, one representative out of two independent experiments with very similar results is shown in each case, with symbols showing the individual values of the biological replicates and the error bars representing SD.

Fig. 3. EpoTg and Tg induce UPR in a dose-dependent manner. A: PC3 cells were seeded in 6-well plates 2 d prior to treatment with the indicated concentrations of EpoTg, Tg, or DMSO control (0.05%). Immunoblotting for XBP1s, ATF4, CHOP, BiP, cleaved PARP (cl-PARP), LC3 (LC3-I denotes free LC3 and LC3-II denotes phosphatidylethanolamine-conjugated LC3), and α-tubulin (tubulin), was performed on samples harvested after 6 h or 24 h of treatment. One representative blot out of 3 independent experiments is shown. The position of molecular weight markers is indicated to the left of the blots. B-G: Quantifications of the immunoblots, normalized to the tubulin loading control in each experiment. All values were subsequently normalized to those obtained with 6 or 24 h treatment with 1500 nM EpoTg (set to 1). *$p<0.05$, **$p<0.01$, ns; not significant, paired Student‘s t-test. The symbols represent values from single experiments, with a separate colour (red, blue, green) for each experiment. Note that statistical tests with comparison to basal levels could only be done for BiP and LC3, since we only for BiP and LC3 could detect quantifiable basal levels in DMSO control-treated cells with high enough signal-to-noise ratios in the immunoblots. This is due to the very low levels of UPR and apoptosis in DMSO control-treated cells.

Fig. 4. Non-cytotoxic, non-UPR-inducing concentrations of EpoTg and Tg strongly deplete releasable ER Ca^{2+}. PC3 cells were seeded in 96-well plates 2 d prior to treatment with the indicated concentrations of EpoTg, Tg, or DMSO control (0.05%). After 1 h, 6 h, 24 h, 48 h and 72 h of treatment, releasable ER Ca^{2+} levels were determined by monitoring cytosolic Ca^{2+} changes with Fura-2 after challenge with ATP. A, B: F_{340}/F_{380} Fura-2 plots of ATP-challenged cells pre-treated for 24 h with EpoTg (A) or Tg (B). All wells received 3 mM EGTA for 60 s, before treatment with 2 µM ATP (indicated by arrow). Mean±SEM of 4

independent experiments. C, D: Area under the curve (AUC) quantifications from the plots obtained after the indicated pre-treatment times and concentrations of EpoTg (C) or Tg (D), normalized to DMSO control (set to 1). Mean±SEM of 4 (3 for 72 h) independent experiments. *p<0.05, **p<0.01, ***p<0.001, ns; not significant, paired Student's t-test compared to DMSO control for each time point.

Fig. 5. Direct measurement of the effects of EpoTg and Tg on ER Ca^{2+} levels. A, B: PC3 cells were seeded in 96-well plates for 2 d followed by a 24 h transfection with the genetically engineered luminal ER-targeted Ca^{2+}-sensing probe G-CEPIA1*er*. Treatment with the indicated final concentrations of EpoTg (A), Tg (B), or DMSO control (0.05%) was added directly to the wells, and declines in G-CEPIA1*er* fluorescence was measured by live-cell fluorescence imaging (IncuCyte ZOOM) every 1 h. ER Ca^{2+} levels are plotted as total fluorescence intensity of G-CEPIA1*er* relative to DMSO control for each condition (to account for changes in G-CEPIA1*er* expression throughout the experiment). Mean±SEM of 3 independent experiments. C, D: Bar plots generated from the values obtained at the 22 h time point in A and B, normalized to values obtained upon an ER Ca^{2+} purge with 5 µM A23187 (a Ca^{2+} ionophore) added at 22 h (this baseline level is set to 1 and indicated by the dashed line). Mean±SEM of 3 independent experiments. The symbols represent values from single experiments, with a separate colour (red, blue, green) for each experiment. *p<0.05, **p<0.01, ***p<0.001, ns; not significant, paired Student's t-test.

Fig. 6. Relationship between EpoTg/Tg-induced ER Ca^{2+} depletion and induction of cell death and UPR in LNCaP cells. A, B: LNCaP cells were seeded in 96-well plates for 2 d followed by a 24 h transfection with a plasmid encoding G-CEPIA1*er*. Treatment with the indicated final concentrations of EpoTg (A), Tg (B), or DMSO control (0.05%) was added directly to the wells, and declines in G-CEPIA1*er* fluorescence was measured by live-cell fluorescence imaging (IncuCyte ZOOM) every 1 h. ER Ca^{2+} levels are plotted as total fluorescence intensity of G-CEPIA1*er* relative to DMSO control. Mean±SD of 3 biological repeats from one representative experiment out of two showing very similar results. C, D: Bar plots generated from the values obtained at the 22 h time point in A and B, normalized to values obtained upon an ER Ca^{2+} purge with 5 µM A23187 added at 22 h (this baseline level is set to 1 and indicated by the dashed line). Mean±SD of the 3 biological repeats, with symbols representing each individual value. E, F: LNCaP cells were seeded in 96-well plates 2 d prior to treatment with the indicated concentrations of EpoTg (E), Tg (F), or DMSO control (0.05%), together with 2.5 µg/ml propidium iodide. Cell death was monitored by live-cell fluorescence imaging (IncuCyte ZOOM) and plotted as ratio of red fluorescent- to total cell confluence after 60 h of treatment. One representative out of two independent experiments with very similar results is shown in each case, with symbols showing the individual values of the biological replicates and the error bars representing SD. G: LNCaP cells were treated with DMSO control (0.05%) or the indicated concentrations of EpoTg or Tg for 6 h or 24 h. Subsequently protein extracts were made and subjected to immunoblotting using antibodies against XBP1s, ATF4, CHOP, BiP, cleaved PARP (cl-PARP), LC3, and α-tubulin, as indicated. One representative blot out of 2 independent experiments with very similar results is shown. The position of molecular weight markers is indicated to the left of the blots.

Fig. 7. Relationship between EGTA-induced ER Ca^{2+} depletion and induction of cell death and UPR in PC3 cells. A: PC3 cells were seeded in 96-well plates for 2 d followed by a 24 h transfection with a plasmid encoding G-CEPIA1*er*. Subsequently, the cells were washed once in Ca^{2+}-free DMEM followed by incubation in Ca^{2+}-free DMEM containing 10% FBS and the indicated final concentrations of EGTA. G-CEPIA1*er* fluorescence was measured by live-cell fluorescence imaging (IncuCyte ZOOM) every 1 h. ER Ca^{2+} levels are plotted as total fluorescence intensity of G-CEPIA1*er* relative to non-EGTA control. Mean±SD of 3 biological repeats from one representative experiment out of two showing very similar results. B: Bar plots generated from the values obtained at the 22 h time point in A, normalized to values obtained upon an ER Ca^{2+} purge with 5 µM A23187 added at 22 h (this baseline level is set to 1 and indicated by the dashed line). Mean±SD of the 3 biological repeats, with symbols representing each individual value. C: PC3 cells were seeded in 6-well plates, and after 2 d the cells were washed once in Ca^{2+}-free DMEM followed by incubation in Ca^{2+}-free DMEM containing 10% FBS and the indicated final concentrations of EGTA for 8 h. Subsequently protein extracts were made and subjected to immunoblotting using antibodies against XBP1s, ATF4, CHOP, BiP, and α-tubulin, as indicated. One representative blot out of 2 independent experiments with very similar results is shown. The position of molecular weight markers is indicated to the left of the blots. D: PC3 cells were seeded in 96-well plates 2 d prior to a wash in Ca^{2+}-free DMEM followed by incubation in Ca^{2+}-free DMEM containing 10% FBS, 2.5 µg/ml propidium iodide, and the indicated final concentrations of EGTA. Cell death was monitored by live-cell fluorescence imaging (IncuCyte ZOOM) and plotted as ratio of red fluorescent- to total cell confluence after 22 h of incubation. Mean±SD of 3 biological repeats from one representative experiment out of two showing very similar results, with symbols representing each individual value.

Fig. 8. High concentrations of Tg are required for inhibition of autophagic sequestration activity. PC3 cells were seeded in 6-well plates 2 d prior to treatment with either DMSO control (0.05%), or the indicated concentrations of Tg for 4 h or 28 h. Subsequently, cells were subjected to an additional 3 h of treatment in EBSS starvation medium supplemented with 150 nM BafA1 (after one wash in EBSS medium), or continued treatment with DMSO control (0.05%) in complete medium. Autophagic sequestration activity is plotted as LDH sequestration rate normalized to the 4 h DMSO pre-treatment control subsequently incubated with EBSS + BafA1 (set to 1). Mean±SEM of 3 independent experiments. *$p<0.05$, **$p<0.01$, ns; not significant, paired Student‘s t-test compared to the 4 h DMSO pre-treatment control subsequently incubated with EBSS + BafA1, unless otherwise indicated.

Fig. 9. Simplified depiction of the major conclusions of the current study. A: Under normal conditions ER Ca^{2+} homeostasis is ensured by the import of Ca^{2+} from the cytosol into the ER lumen by SERCA pumps, and a basal level of Ca^{2+} leak through Ca^{2+} leak channels and IP3R. Protein folding is efficient, and thus the unfolded protein response (UPR) sensors PERK, IRE1 and ATF6 are not activated. B: Treatment with intermediate concentrations of SERCA inhibitors results in a strong block in SERCA activity and a sustained depletion of the bulk of ER Ca^{2+} through Ca^{2+} leak mechanisms. This leads to reduced cell proliferation, but remarkably, the UPR is not activated and the cells do not undergo cell death. Moreover, starvation-induced

bulk autophagy is still fully supported. C: In cells treated with high concentrations of SERCA inhibitors, the UPR is activated in a strong and sustained manner, and this leads to apoptotic cell death. Moreover, bulk autophagy is inhibited at the autophagosome formation step. The UPR is most likely induced under these conditions because the ER Ca^{2+} levels decrease to levels that are incompatible with efficient protein folding, leading to accumulation of unfolded proteins and activation of the ER stress sensors and UPR initiators PERK, IRE1 and ATF6. This critical decrease of ER Ca^{2+} levels in areas of the ER that perform protein folding and contain the ER stress sensors may simply be the result of a general depletion of ER Ca^{2+} which is stronger than the situation shown in B. This would imply that protein folding is well maintained even under conditions of very low ER Ca^{2+} levels (as in B). Alternatively, it may be that the areas of ER which perform protein folding and contain the ER stress sensors are more resistant to ER Ca^{2+} drainage than the bulk of ER, and therefore the critical decrease of ER Ca^{2+} levels in those areas requires higher SERCA inhibitor concentrations. This possibility is indicated by the hypothesized less severe effect of the SERCA inhibitors on ER Ca^{2+} depletion in the ER subdomain that contains the ER stress sensors (in B), and the accumulation of unfolded proteins upon a further decrease in Ca^{2+} levels in that subdomain in cells treated with high concentrations of SERCA inhibitors (in C).

Supplementary Information

Fig. S1. Dose-dependency of EpoTg- and Tg-induced cell death. Bar plots from the values at the 60 h time point in Fig. 2A and B. Mean±SEM of 3 independent experiments. *p<0.05, **p<0.01, ns; not significant, paired Student‘s t-test.

Fig. S2. High concentrations of EpoTg or Tg induce caspase-dependent cell death, whereas lower concentrations produce cytostatic effects. A, B: PC3 cells were seeded in 96-well plates 2 d prior to treatment with the indicated concentrations of EpoTg (A), Tg (B), or DMSO control (0.05%), together with 2.5 µg/ml propidium iodide, in the absence (upper panels) or presence (lower panels) of 50 µM Z-VAD-FMK (zVAD). Cell death was monitored by live-cell fluorescence imaging (IncuCyte ZOOM) every 3 h. Relative cell death is plotted over time as ratio of red fluorescent- to total cell confluence, normalized to the average ratio of each experiment (as in Fig. 2A and B). Mean±SD of 3 biological repeats from one representative experiment out of two showing very similar results. C, D: Relative cell confluency (recorded by live-cell phase-contrast imaging in the same experiments as described in A and B) plotted over time and normalized to the confluency of each condition at 0 h. Mean±SD of 3 biological repeats from one representative experiment out of two showing very similar results. E, F: PC3 cells were treated with the indicated concentrations of EpoTg (E) or Tg (F) in the absence or presence of 50 µM Z-VAD-FMK (zVAD) or DMSO control (0.05%), and after 44 h the number of viable cells was assessed by the CellTiter 96 AQ_{ueous} One Solution assay, normalized to the DMSO control-treated cells in the absence of EpoTg/Tg (set to 1). One representative out of two independent experiments with very similar results is shown in each case, with symbols showing the individual values of the biological replicates and the error bars representing SD.

Fig. S3. Non-cytotoxic, non-UPR-inducing concentrations of EpoTg and Tg strongly deplete high-dose Tg-releasable ER Ca^{2+}. PC3 cells were seeded in 96-well plates 2 d prior to treatment with the indicated concentrations of EpoTg, Tg, or DMSO control (0.05%). After 1 h, 6 h, 24 h, 48 h and 72 h of treatment, releasable ER Ca^{2+} levels were determined by monitoring cytosolic Ca^{2+} changes with Fura-2 after challenge with high-dose Tg (1 µM). A, B: F_{340}/F_{380} Fura-2 plots of high-dose Tg-challenged cells pre-treated for 24 h with EpoTg (A) or Tg (B). All wells received 3 mM EGTA for 60 s, before treatment with 1 µM Tg (indicated by arrow). Mean±SEM of 4 independent experiments. C, D: Area under the curve (AUC) quantifications from the plots obtained after the indicated pre-treatment times and concentrations of EpoTg (C) or Tg (D), normalized to DMSO control (set to 1). Mean±SEM of 4 (3 for 72 h) independent experiments. *p<0.05, **p<0.01, ***p<0.001, ns; not significant, paired Student‘s t-test compared to DMSO control for each time point.

Fig. S4. Non-cytotoxic, non-UPR-inducing concentrations of EpoTg strongly deplete ionomycin-releasable ER Ca^{2+}. PC3 cells were seeded in 96-well plates 2 d prior to treatment with the indicated concentrations of EpoTg, or DMSO control (0.05%). After 1 h, 6 h, and 72 h of treatment, releasable ER Ca^{2+} levels were determined by monitoring cytosolic Ca^{2+} changes with Fura-2 after challenge with the Ca^{2+} ionophore ionomycin (2 µM). A: F_{340}/F_{380} Fura-2 plots of ionomycin-challenged cells pre-treated for 6 h with EpoTg. All wells received 3 mM EGTA for 60 s, before treatment with ionomycin (indicated by arrow). Mean±absolute

deviation of duplicate biological replicates from one representative experiment out of two. B: Area under the curve (AUC) quantifications from the plots obtained after the indicated pre-treatment times and concentrations of EpoTg, normalized to DMSO control (set to 1). Mean±absolute deviation of duplicate biological replicates from one representative experiment out of two.

Fig. S5. G-CEPIA1*er* co-localizes with ER-Tracker red. PC3 cells were seeded in 96-well plates for 2 d followed by a 24 h transfection with an expression plasmid encoding the genetically engineered luminal ER-targeted G-CEPIA1*er*. Subsequently, cells were stained with 0.8 µM ER-Tracker Red for 20 min at 37°C, and analysed with an Axio Vert.A1 microscope. Shown is a representative image comparing the brightfield image (left), the green fluorescence from G-CEPIA1*er* (middle) and the red fluorescence from ER-Tracker Red (right). As expected, the signals from G-CEPIA1*er* and ER-Tracker Red are strongly overlapping, indicating a high degree of co-localization. Scale bar = 10 µm.

Fig. S6. Overview of the relationship between ER Ca^{2+} levels, UPR and cell death. A: Expected relationship between ER Ca^{2+} levels versus induction of UPR and cell death if UPR induction and cell death gradually increase in a linear manner as the ER Ca^{2+} levels decrease. B: Summary of our experimental data obtained with EpoTg in PC3 cells. Plotted are: (i) relative ER Ca^{2+} levels as assessed with G-CEPIA1*er* after 22 h of treatment in Fig. 5 (set to 100% for DMSO control), (ii) relative amounts of ATP/Tg-releasable Ca^{2+} after 24 h of treatment as assessed by the Fura-2 measurements in Fig. 4 and Fig. S3 (set to 100% for DMSO control), (iii) Relative UPR levels assessed by averaging the quantifications of ATF4, CHOP, BiP protein levels at 24 h in Fig. 3 (setting the value obtained with the highest drug concentration to 100%), and (iv) relative values of cell death obtained from the propidium iodide measurements at 60 h in Fig. S1 (setting the value obtained with the highest drug concentration to 100%). Mean±SEM of 3-4 independent experiments. C: Summary of our experimental data obtained with Tg in PC3 cells, expressed in the same manner as in B.

Fig. S7. Low concentrations of EpoTg or Tg produce cytostatic effects in LNCaP cells, whereas high concentrations induce caspase-dependent cell death. A, B: LNCaP cells were seeded in 96-well plates 2 d prior to treatment with the indicated concentrations of EpoTg (A), Tg (B), or DMSO control (0.05%). Cell confluence was monitored by live-cell phase-contrast imaging (IncuCyte ZOOM) every 3 h, and plotted over time, normalized to the confluency of each condition at 0 h. Mean±SD of 3 biological repeats from one representative experiment out of two showing very similar results. C, D: LNCaP cells were treated with the indicated concentrations of EpoTg (C) or Tg (D) in the absence or presence of 50 µM Z-VAD-FMK (zVAD) or DMSO control (0.05%), together with 2.5 µg/ml propidium iodide. Cell death was monitored by live-cell phase-contrast and fluorescence imaging (IncuCyte ZOOM) and plotted as ratio of red fluorescent- to total cell confluence after 60 h of treatment. One representative out of two independent experiments with very similar results is shown in each case, with symbols showing the individual values of the biological replicates and the error bars representing SD.

Fig. S8. High concentrations of Tg are required for inhibition of autophagic degradation activity. PC3 cells were seeded in 24-well plates, and proteins were radiolabelled with ^{14}C valine for 2 d in complete medium prior to wash-out of unincorporated ^{14}C-valine, and an 18 h chase period in complete medium containing a surplus of cold (non-radioactive) valine and either DMSO control (0.05%) or the indicated concentrations of Tg for 18 h. Subsequently, short-lived protein degradation products were washed out, and cells were subjected to 3 h of treatment in EBSS starvation medium or incubation in complete medium (CM). Autophagic degradation activity is plotted as the long-lived protein degradation rate normalized to DMSO pre-treated cells subsequently incubated with EBSS (set to 1). Mean±SD of 3 biological replicates, with symbols showing the individual values of the biological replicates.

Fig 1

A

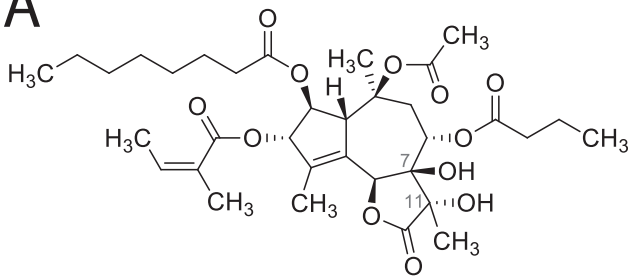

Thapsigargin (Tg)

B

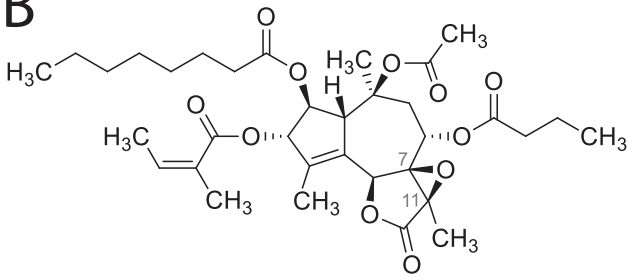

Thapsigargin epoxide (EpoTg)

Fig 2

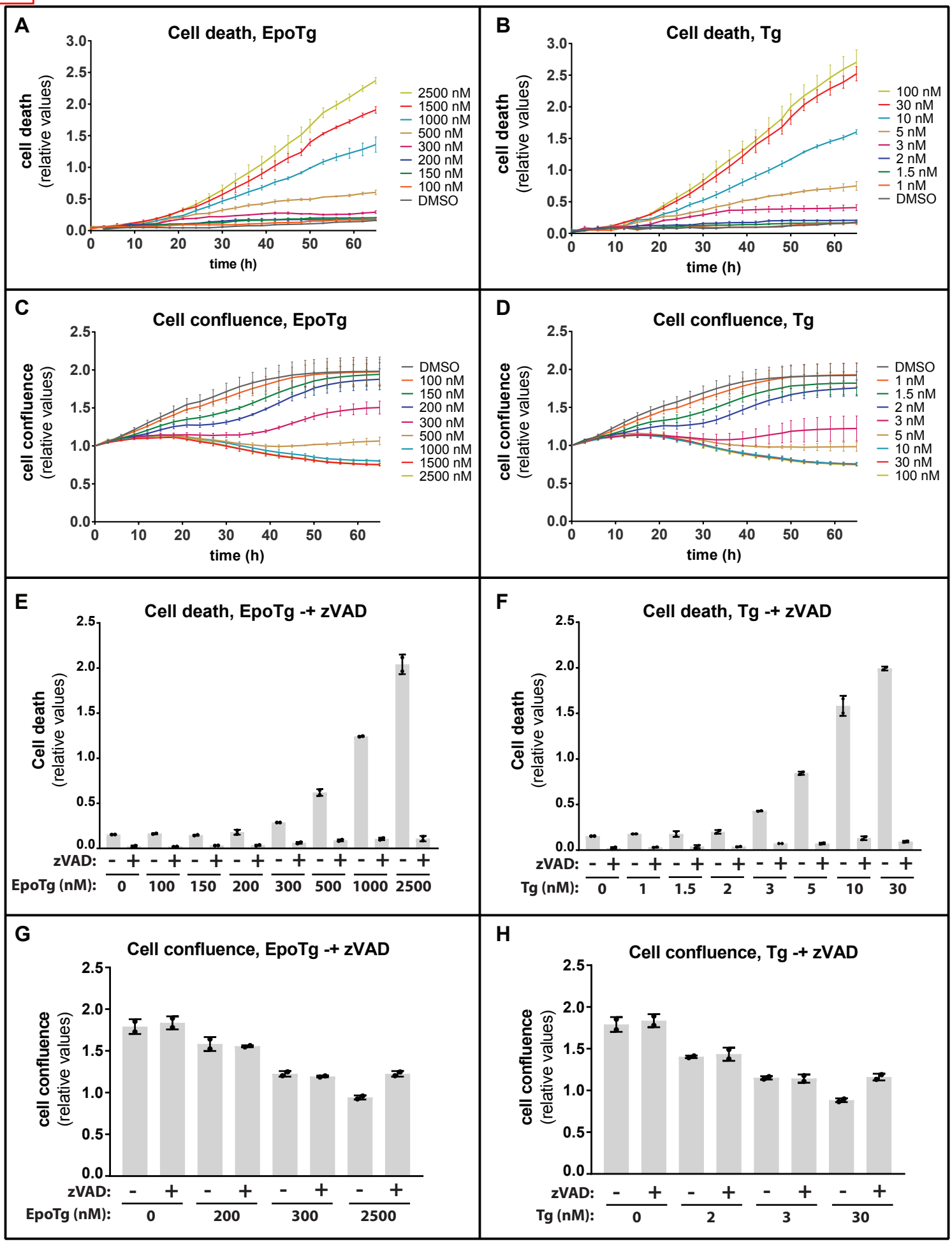
A
Cell death, EpoTg
cell death (relative values)
time (h)
2500 nM
1500 nM
1000 nM
500 nM
300 nM
200 nM
150 nM
100 nM
DMSO
B
Cell death, Tg
cell death (relative values)
time (h)
100 nM
30 nM
10 nM
5 nM
3 nM
2 nM
1.5 nM
1 nM
DMSO
C
Cell confluence, EpoTg
cell confluence (relative values)
time (h)
DMSO
100 nM
150 nM
200 nM
300 nM
500 nM
1000 nM
1500 nM
2500 nM
D
Cell confluence, Tg
cell confluence (relative values)
time (h)
DMSO
1 nM
1.5 nM
2 nM
3 nM
5 nM
10 nM
30 nM
100 nM
E
Cell death, EpoTg -+ zVAD
Cell death (relative values)
zVAD:
EpoTg (nM):
0
100
150
200
300
500
1000
2500
F
Cell death, Tg -+ zVAD
Cell death (relative values)
zVAD:
Tg (nM):
0
1
1.5
2
3
5
10
30
G
Cell confluence, EpoTg -+ zVAD
cell confluence (relative values)
zVAD:
EpoTg (nM):
0
200
300
2500
H
Cell confluence, Tg -+ zVAD
cell confluence (relative values)
zVAD:
Tg (nM):
0
2
3
30

Fig 3

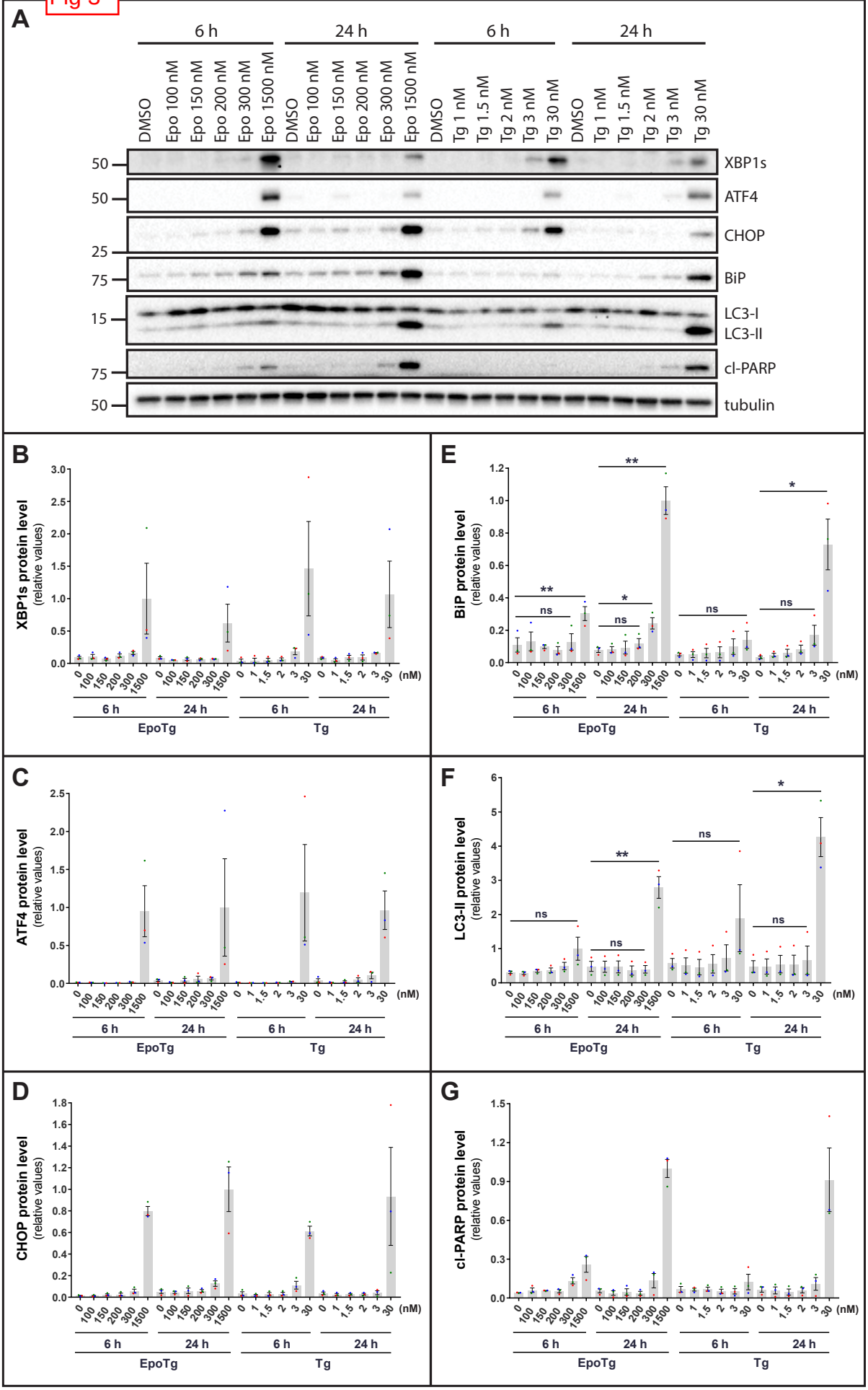
A
6 h
24 h
6 h
24 h
DMSO
Epo 100 nM
Epo 150 nM
Epo 200 nM
Epo 300 nM
Epo 1500 nM
DMSO
Epo 100 nM
Epo 150 nM
Epo 200 nM
Epo 300 nM
Epo 1500 nM
DMSO
Tg 1 nM
Tg 1.5 nM
Tg 2 nM
Tg 3 nM
Tg 30 nM
DMSO
Tg 1 nM
Tg 1.5 nM
Tg 2 nM
Tg 3 nM
Tg 30 nM
50
50
25
75
15
75
50
XBP1s
ATF4
CHOP
BiP
LC3-I
LC3-II
cl-PARP
tubulin
B
XBP1s protein level
(relative values)
E
BiP protein level
(relative values)
C
ATF4 protein level
(relative values)
F
LC3-II protein level
(relative values)
D
CHOP protein level
(relative values)
G
cl-PARP protein level
(relative values)
(nM)
6 h
24 h
6 h
24 h
EpoTg
Tg
ns
*
**

Fig 4

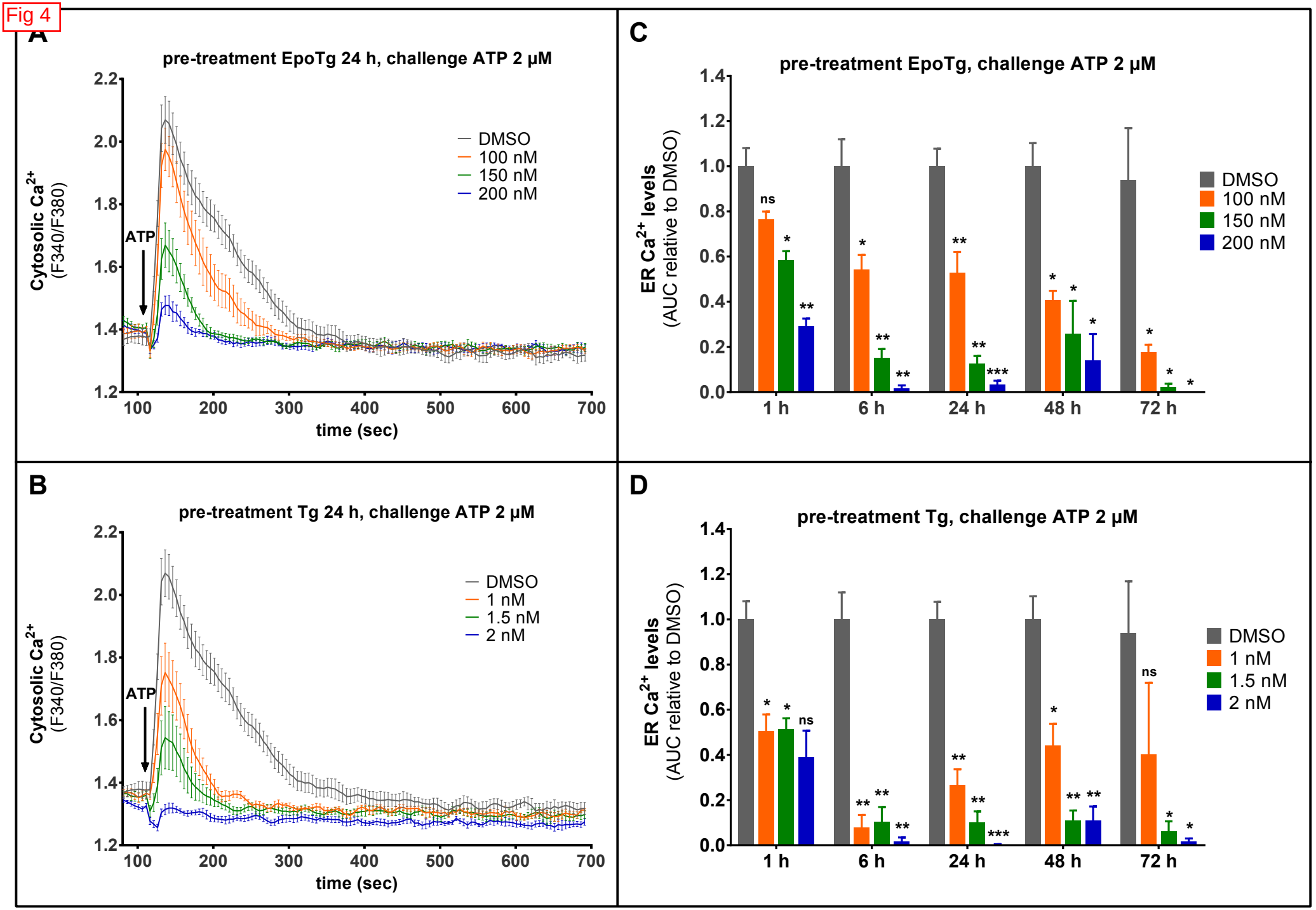
A
pre-treatment EpoTg 24 h, challenge ATP 2 μM
Cytosolic Ca2+ (F340/F380)
ATP
DMSO
100 nM
150 nM
200 nM
time (sec)
B
pre-treatment Tg 24 h, challenge ATP 2 μM
Cytosolic Ca2+ (F340/F380)
ATP
DMSO
1 nM
1.5 nM
2 nM
time (sec)
C
pre-treatment EpoTg, challenge ATP 2 μM
ER Ca2+ levels (AUC relative to DMSO)
DMSO
100 nM
150 nM
200 nM
1 h
6 h
24 h
48 h
72 h
D
pre-treatment Tg, challenge ATP 2 μM
ER Ca2+ levels (AUC relative to DMSO)
DMSO
1 nM
1.5 nM
2 nM
1 h
6 h
24 h
48 h
72 h

Fig 5

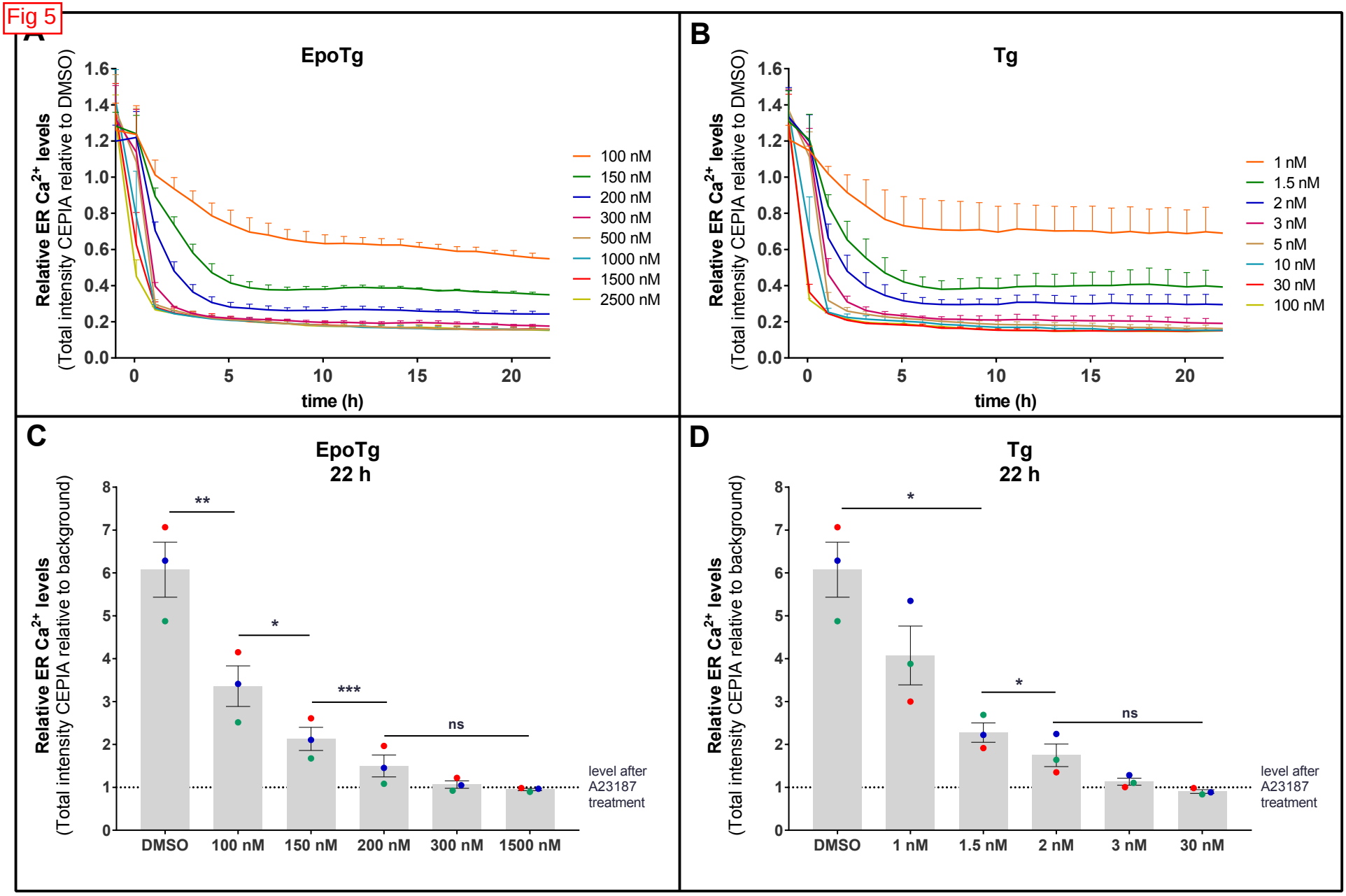
A
EpoTg
Relative ER Ca2+ levels
(Total intensity CEPIA relative to DMSO)
time (h)
100 nM
150 nM
200 nM
300 nM
500 nM
1000 nM
1500 nM
2500 nM
B
Tg
Relative ER Ca2+ levels
(Total intensity CEPIA relative to DMSO)
time (h)
1 nM
1.5 nM
2 nM
3 nM
5 nM
10 nM
30 nM
100 nM
C
EpoTg
22 h
Relative ER Ca2+ levels
(Total intensity CEPIA relative to background)
**
*
***
ns
level after A23187 treatment
DMSO
100 nM
150 nM
200 nM
300 nM
1500 nM
D
Tg
22 h
Relative ER Ca2+ levels
(Total intensity CEPIA relative to background)
*
*
ns
level after A23187 treatment
DMSO
1 nM
1.5 nM
2 nM
3 nM
30 nM

Fig 6

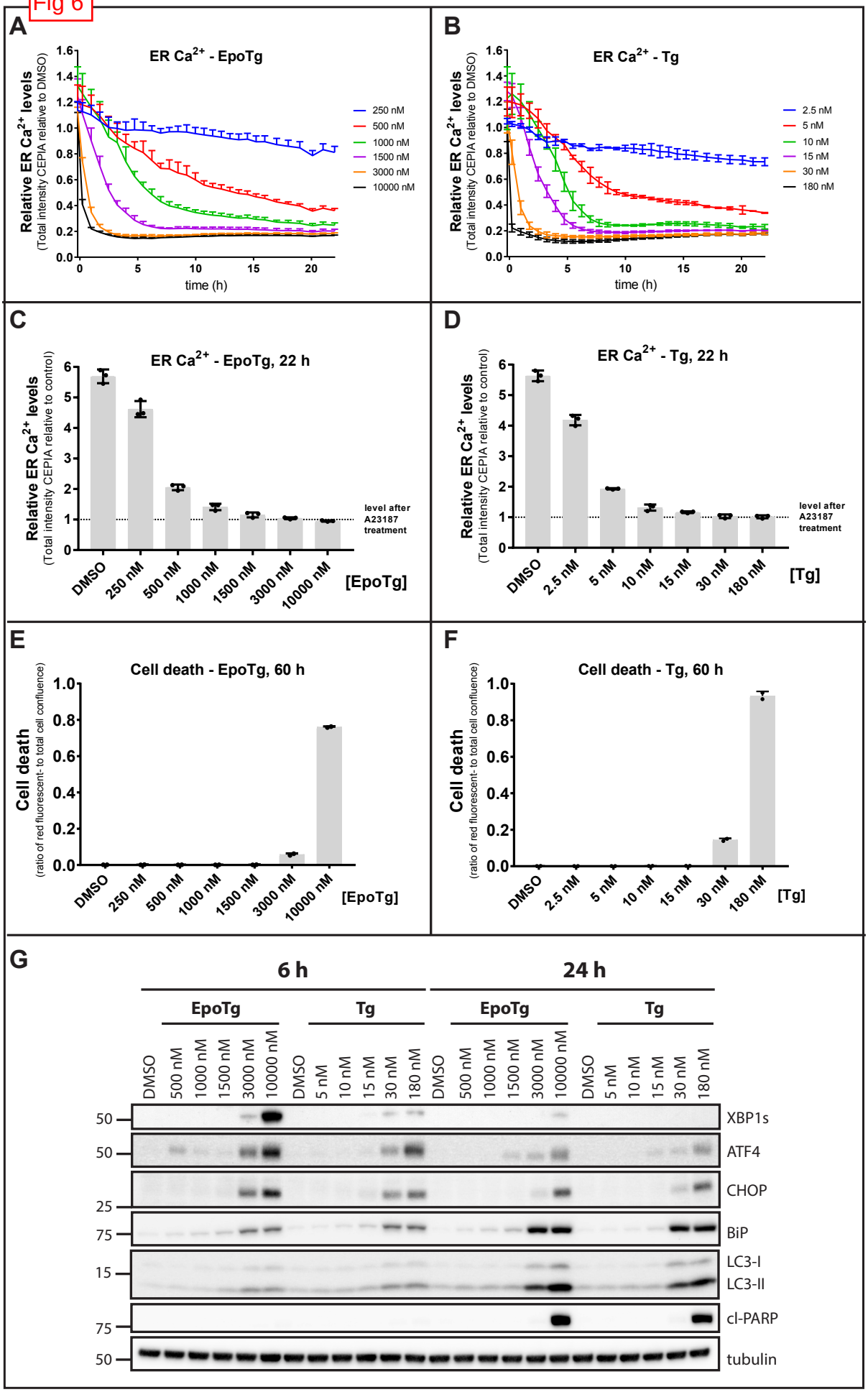
A
ER Ca2+ - EpoTg
Relative ER Ca2+ levels
(Total intensity CEPIA relative to DMSO)
time (h)
250 nM
500 nM
1000 nM
1500 nM
3000 nM
10000 nM
B
ER Ca2+ - Tg
Relative ER Ca2+ levels
(Total intensity CEPIA relative to DMSO)
time (h)
2.5 nM
5 nM
10 nM
15 nM
30 nM
180 nM
C
ER Ca2+ - EpoTg, 22 h
Relative ER Ca2+ levels
(Total intensity CEPIA relative to control)
level after A23187 treatment
DMSO
250 nM
500 nM
1000 nM
1500 nM
3000 nM
10000 nM
[EpoTg]
D
ER Ca2+ - Tg, 22 h
Relative ER Ca2+ levels
(Total intensity CEPIA relative to control)
level after A23187 treatment
DMSO
2.5 nM
5 nM
10 nM
15 nM
30 nM
180 nM
[Tg]
E
Cell death - EpoTg, 60 h
Cell death
(ratio of red fluorescent- to total cell confluence)
DMSO
250 nM
500 nM
1000 nM
1500 nM
3000 nM
10000 nM
[EpoTg]
F
Cell death - Tg, 60 h
Cell death
(ratio of red fluorescent- to total cell confluence)
DMSO
2.5 nM
5 nM
10 nM
15 nM
30 nM
180 nM
[Tg]
G
6 h
24 h
EpoTg
Tg
EpoTg
Tg
DMSO
500 nM
1000 nM
1500 nM
3000 nM
10000 nM
DMSO
5 nM
10 nM
15 nM
30 nM
180 nM
DMSO
500 nM
1000 nM
1500 nM
3000 nM
10000 nM
DMSO
5 nM
10 nM
15 nM
30 nM
180 nM
50
50
25
75
15
75
50
XBP1s
ATF4
CHOP
BiP
LC3-I
LC3-II
cl-PARP
tubulin

Fig 7

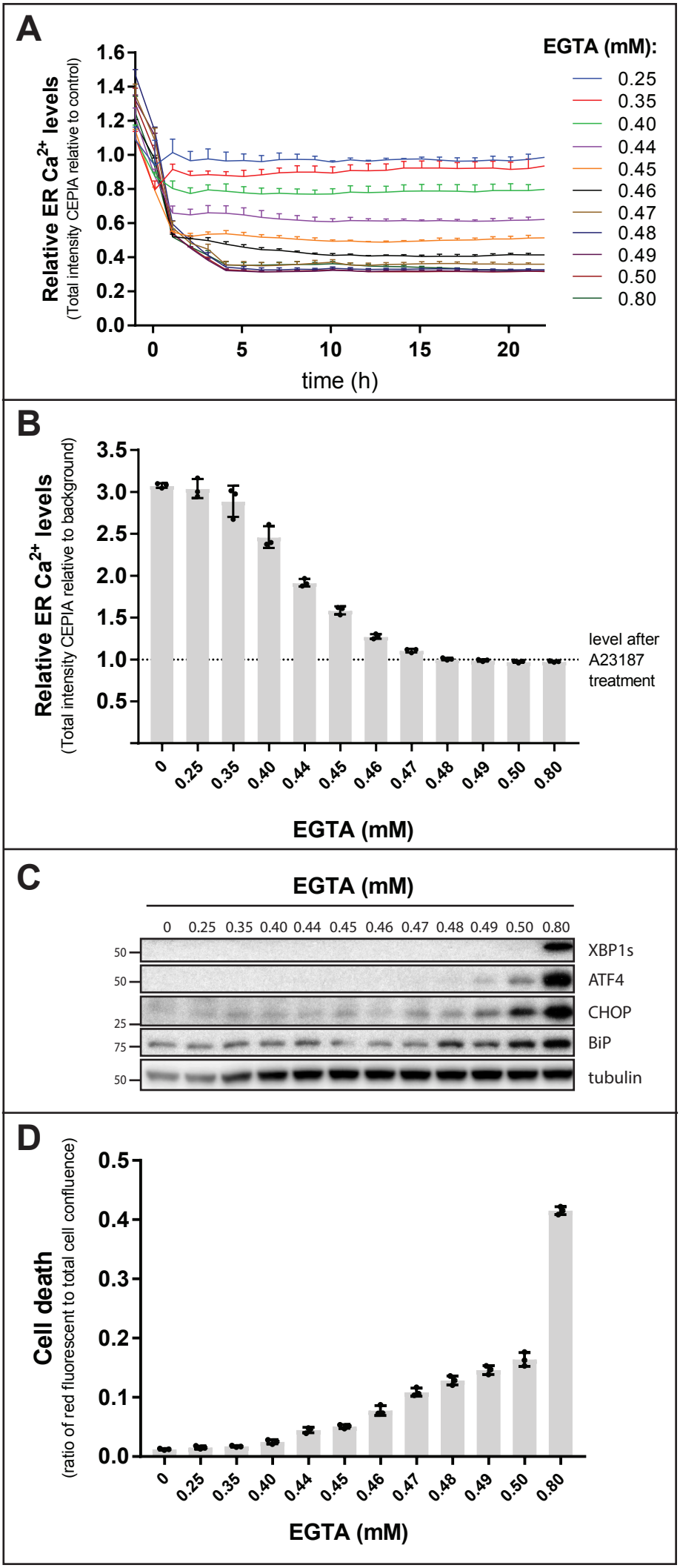
A
Relative ER Ca2+ levels
(Total intensity CEPIA relative to control)
EGTA (mM):
0.25
0.35
0.40
0.44
0.45
0.46
0.47
0.48
0.49
0.50
0.80
time (h)
B
Relative ER Ca2+ levels
(Total intensity CEPIA relative to background)
level after A23187 treatment
EGTA (mM)
C
EGTA (mM)
0 0.25 0.35 0.40 0.44 0.45 0.46 0.47 0.48 0.49 0.50 0.80
XBP1s
ATF4
CHOP
BiP
tubulin
D
Cell death
(ratio of red fluorescent to total cell confluence)
EGTA (mM)

Fig 8

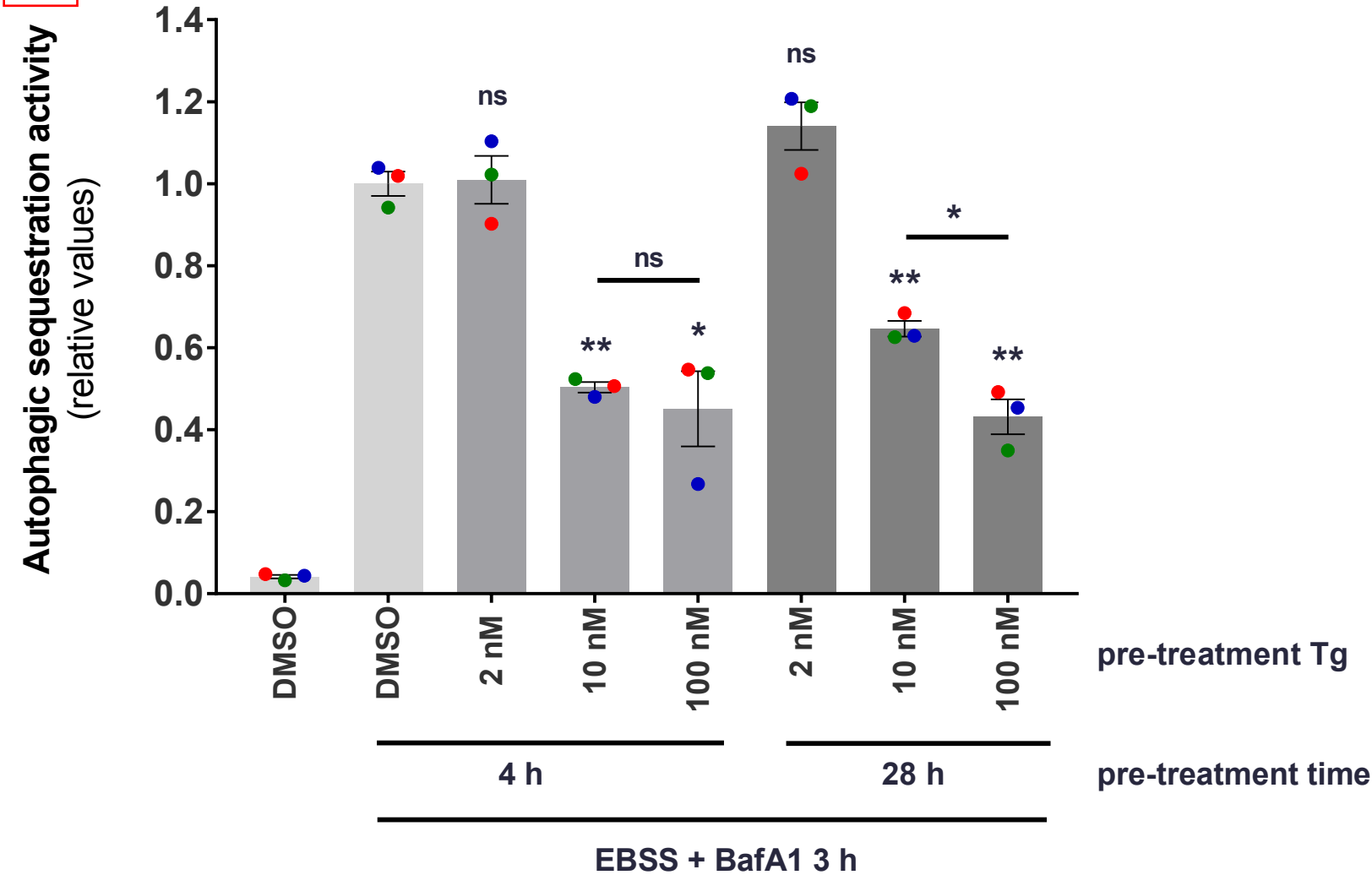
Autophagic sequestration activity
(relative values)
1.4
1.2
1.0
0.8
0.6
0.4
0.2
0.0
ns
ns
ns
*
**
*
**
**
DMSO
DMSO
2 nM
10 nM
100 nM
2 nM
10 nM
100 nM
pre-treatment Tg
4 h
28 h
pre-treatment time
EBSS + BafA1 3 h

Fig 9

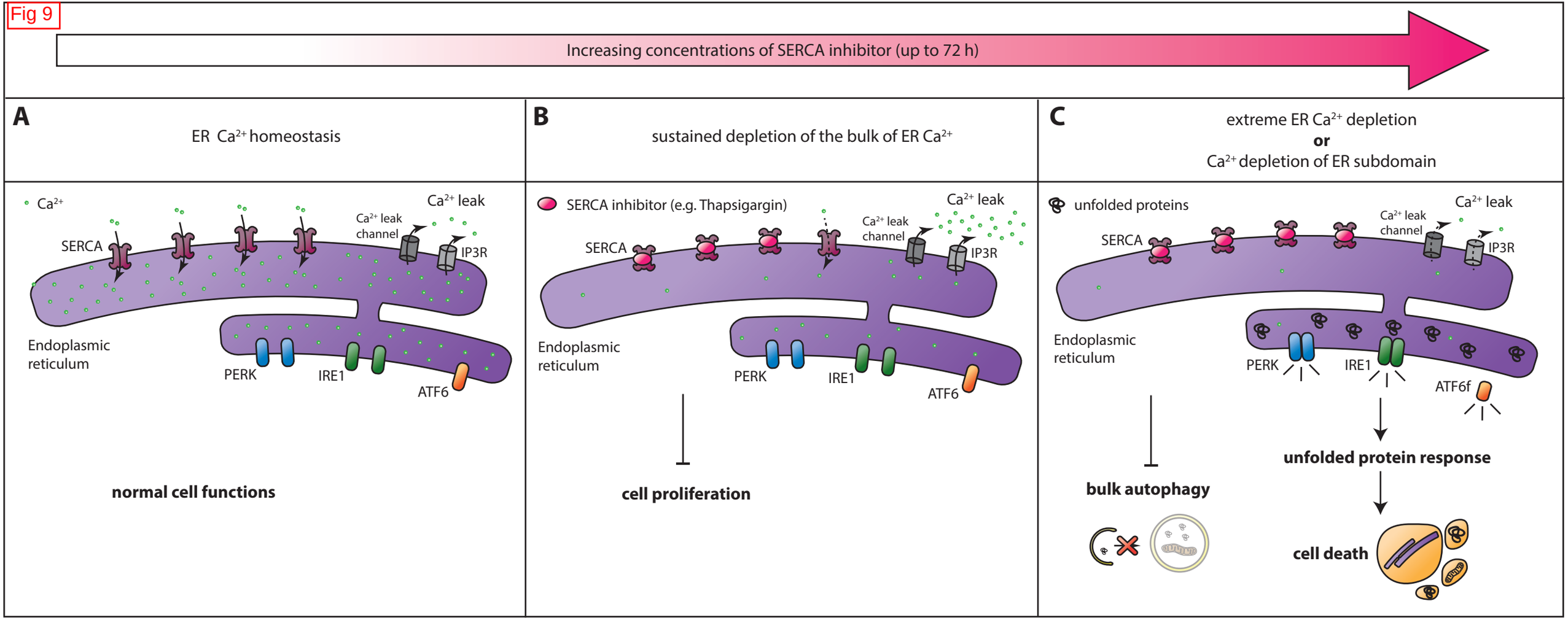
Increasing concentrations of SERCA inhibitor (up to 72 h)
A
ER Ca2+ homeostasis
Ca2+
Ca2+ leak
Ca2+ leak channel
SERCA
IP3R
Endoplasmic reticulum
PERK
IRE1
ATF6
normal cell functions
B
sustained depletion of the bulk of ER Ca2+
SERCA inhibitor (e.g. Thapsigargin)
Ca2+ leak
Ca2+ leak channel
SERCA
IP3R
Endoplasmic reticulum
PERK
IRE1
ATF6
cell proliferation
C
extreme ER Ca2+ depletion
or
Ca2+ depletion of ER subdomain
unfolded proteins
Ca2+ leak
Ca2+ leak channel
SERCA
IP3R
Endoplasmic reticulum
PERK
IRE1
ATF6f
unfolded protein response
bulk autophagy
cell death

SupFig 1

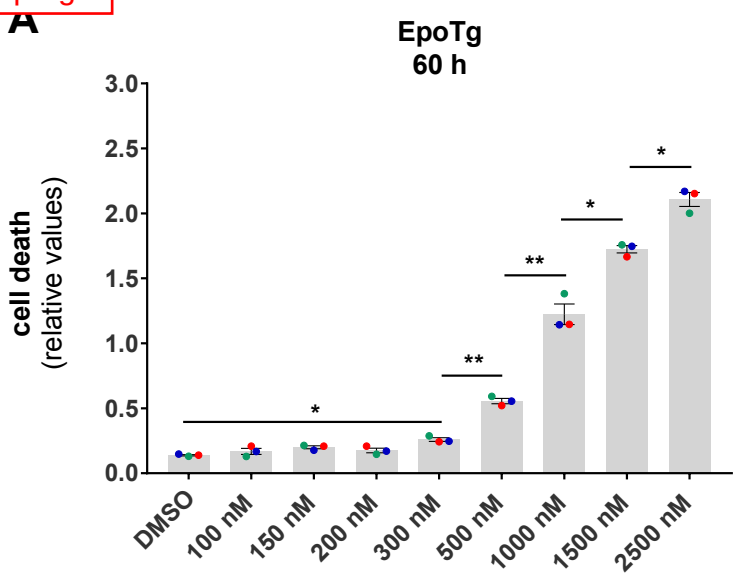
A
EpoTg
60 h
cell death
(relative values)
3.0
2.5
2.0
1.5
1.0
0.5
0.0
*
**
**
*
*
DMSO
100 nM
150 nM
200 nM
300 nM
500 nM
1000 nM
1500 nM
2500 nM

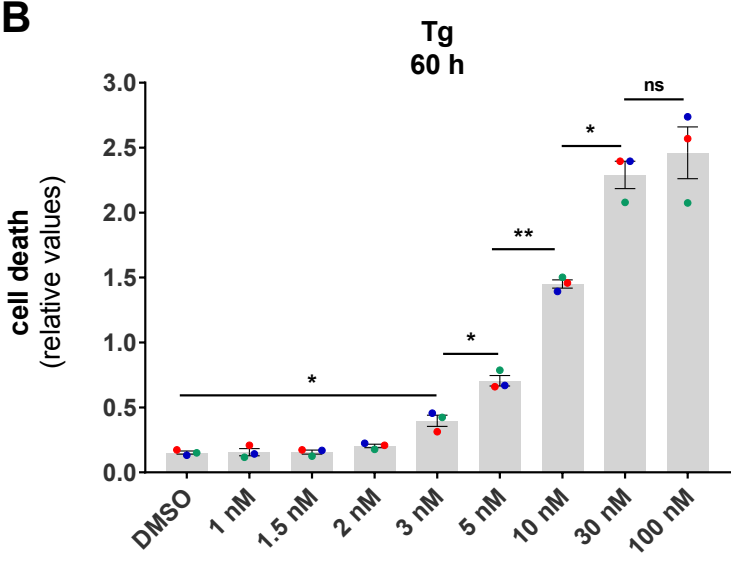
B
Tg
60 h
cell death
(relative values)
3.0
2.5
2.0
1.5
1.0
0.5
0.0
*
*
**
*
ns
DMSO
1 nM
1.5 nM
2 nM
3 nM
5 nM
10 nM
30 nM
100 nM

SupFig 2

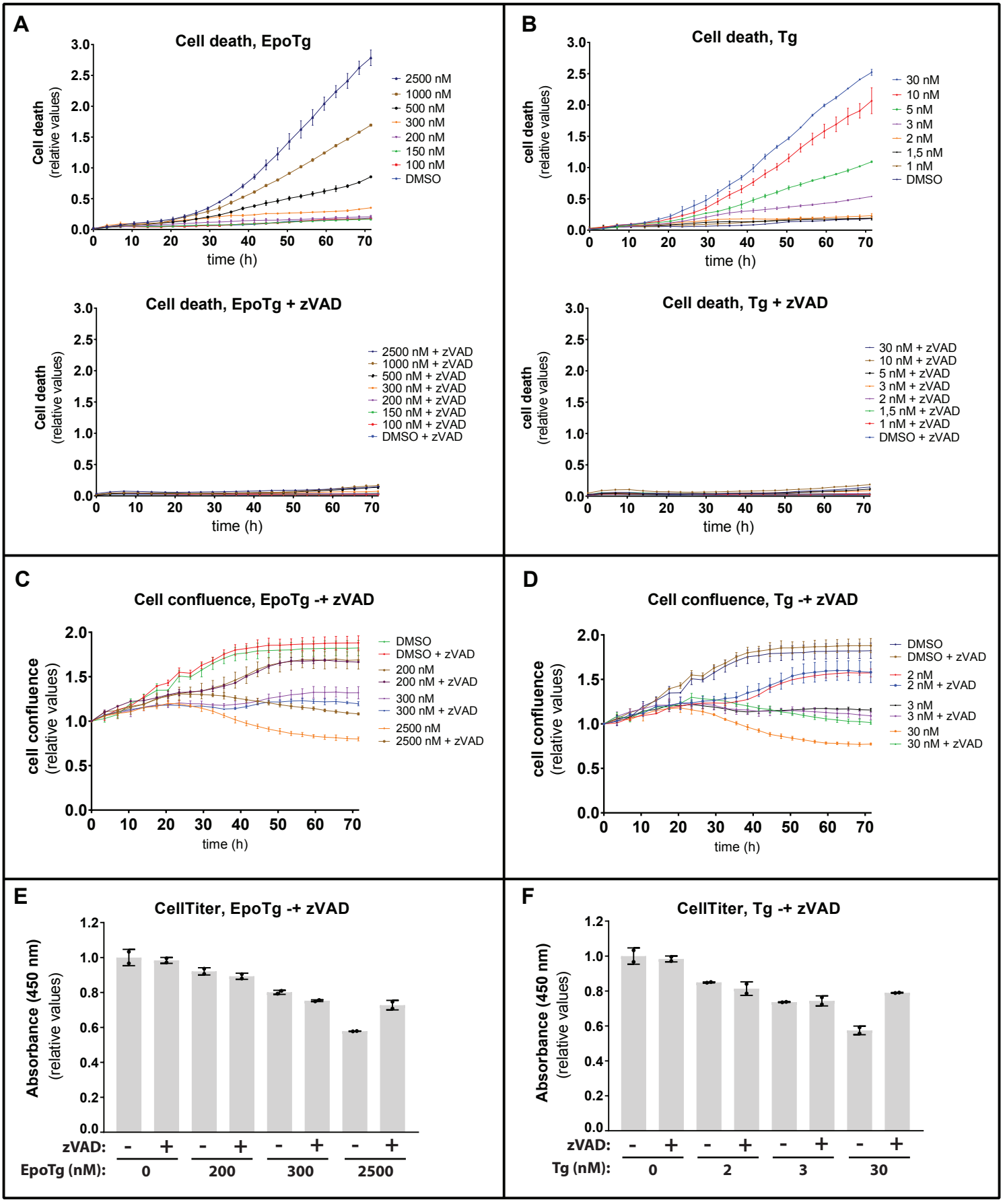
A
Cell death, EpoTg
Cell death (relative values)
time (h)
2500 nM
1000 nM
500 nM
300 nM
200 nM
150 nM
100 nM
DMSO
Cell death, EpoTg + zVAD
2500 nM + zVAD
1000 nM + zVAD
500 nM + zVAD
300 nM + zVAD
200 nM + zVAD
150 nM + zVAD
100 nM + zVAD
DMSO + zVAD
B
Cell death, Tg
30 nM
10 nM
5 nM
3 nM
2 nM
1,5 nM
1 nM
DMSO
Cell death, Tg + zVAD
30 nM + zVAD
10 nM + zVAD
5 nM + zVAD
3 nM + zVAD
2 nM + zVAD
1,5 nM + zVAD
1 nM + zVAD
DMSO + zVAD
C
Cell confluence, EpoTg -+ zVAD
cell confluence (relative values)
DMSO
DMSO + zVAD
200 nM
200 nM + zVAD
300 nM
300 nM + zVAD
2500 nM
2500 nM + zVAD
D
Cell confluence, Tg -+ zVAD
DMSO
DMSO + zVAD
2 nM
2 nM + zVAD
3 nM
3 nM + zVAD
30 nM
30 nM + zVAD
E
CellTiter, EpoTg -+ zVAD
Absorbance (450 nm) (relative values)
zVAD:
EpoTg (nM):
0
200
300
2500
F
CellTiter, Tg -+ zVAD
zVAD:
Tg (nM):
0
2
3
30

SupFig 3

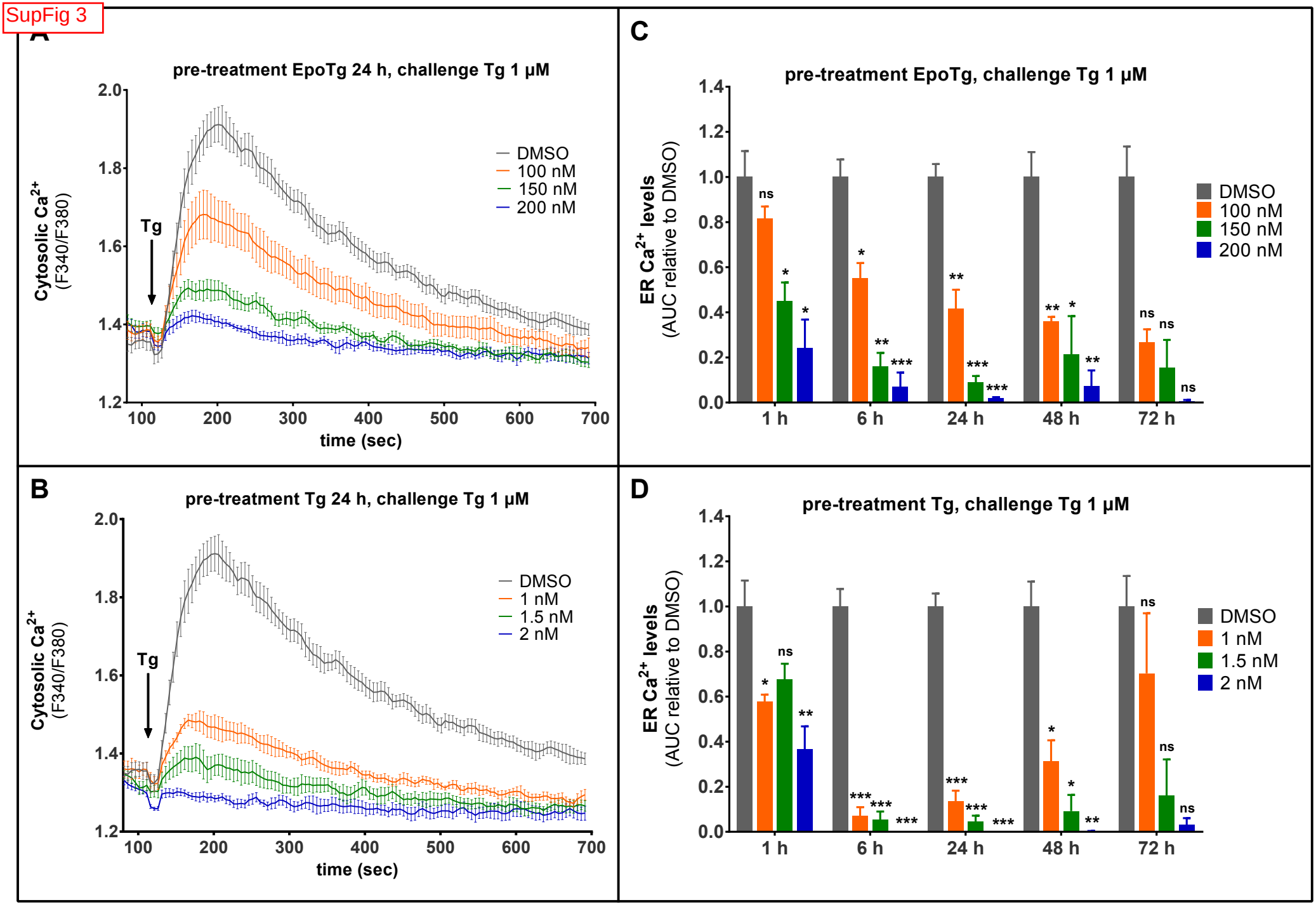
A
pre-treatment EpoTg 24 h, challenge Tg 1 µM
Cytosolic Ca2+ (F340/F380)
time (sec)
Tg
DMSO
100 nM
150 nM
200 nM
B
pre-treatment Tg 24 h, challenge Tg 1 µM
Cytosolic Ca2+ (F340/F380)
time (sec)
Tg
DMSO
1 nM
1.5 nM
2 nM
C
pre-treatment EpoTg, challenge Tg 1 µM
ER Ca2+ levels (AUC relative to DMSO)
1 h
6 h
24 h
48 h
72 h
DMSO
100 nM
150 nM
200 nM
D
pre-treatment Tg, challenge Tg 1 µM
ER Ca2+ levels (AUC relative to DMSO)
1 h
6 h
24 h
48 h
72 h
DMSO
1 nM
1.5 nM
2 nM

SupFig 4

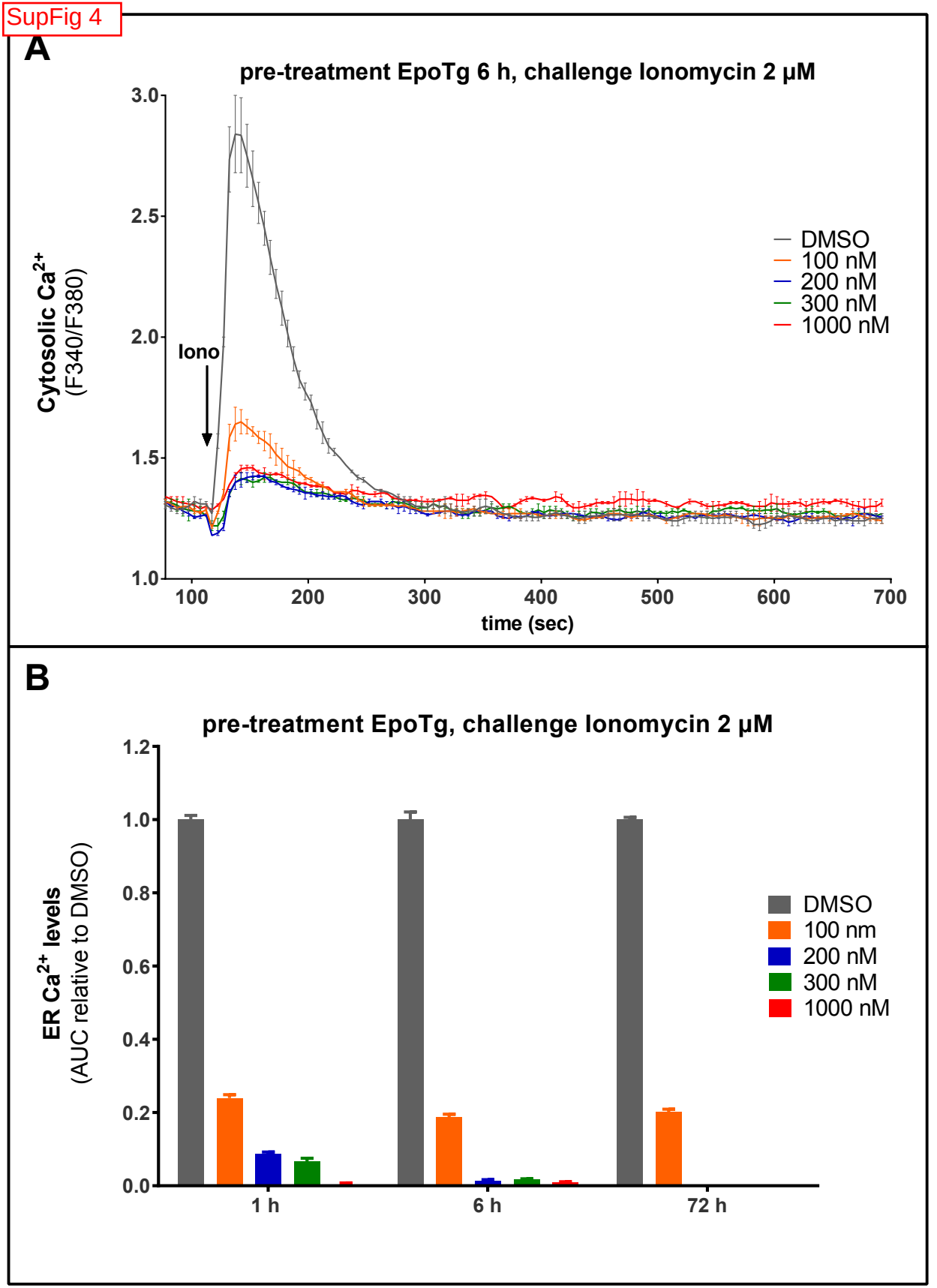
A
pre-treatment EpoTg 6 h, challenge Ionomycin 2 µM
Cytosolic Ca2+
(F340/F380)
3.0
2.5
2.0
1.5
1.0
Iono
DMSO
100 nM
200 nM
300 nM
1000 nM
100
200
300
400
500
600
700
time (sec)
B
pre-treatment EpoTg, challenge Ionomycin 2 µM
ER Ca2+ levels
(AUC relative to DMSO)
1.2
1.0
0.8
0.6
0.4
0.2
0.0
DMSO
100 nm
200 nM
300 nM
1000 nM
1 h
6 h
72 h

SupFig 5

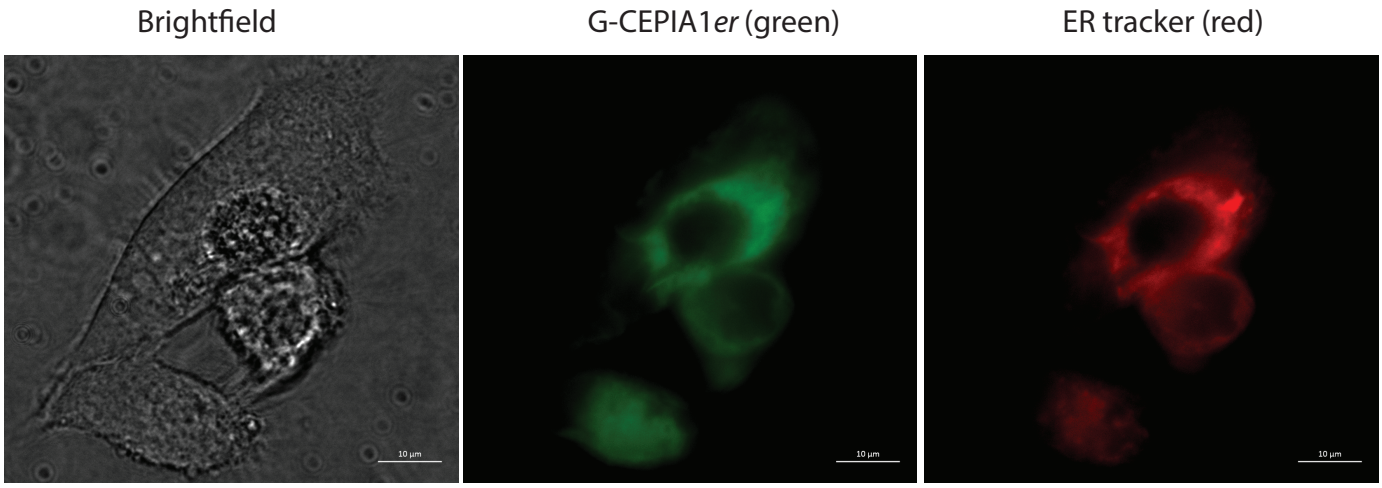

SupFig 6

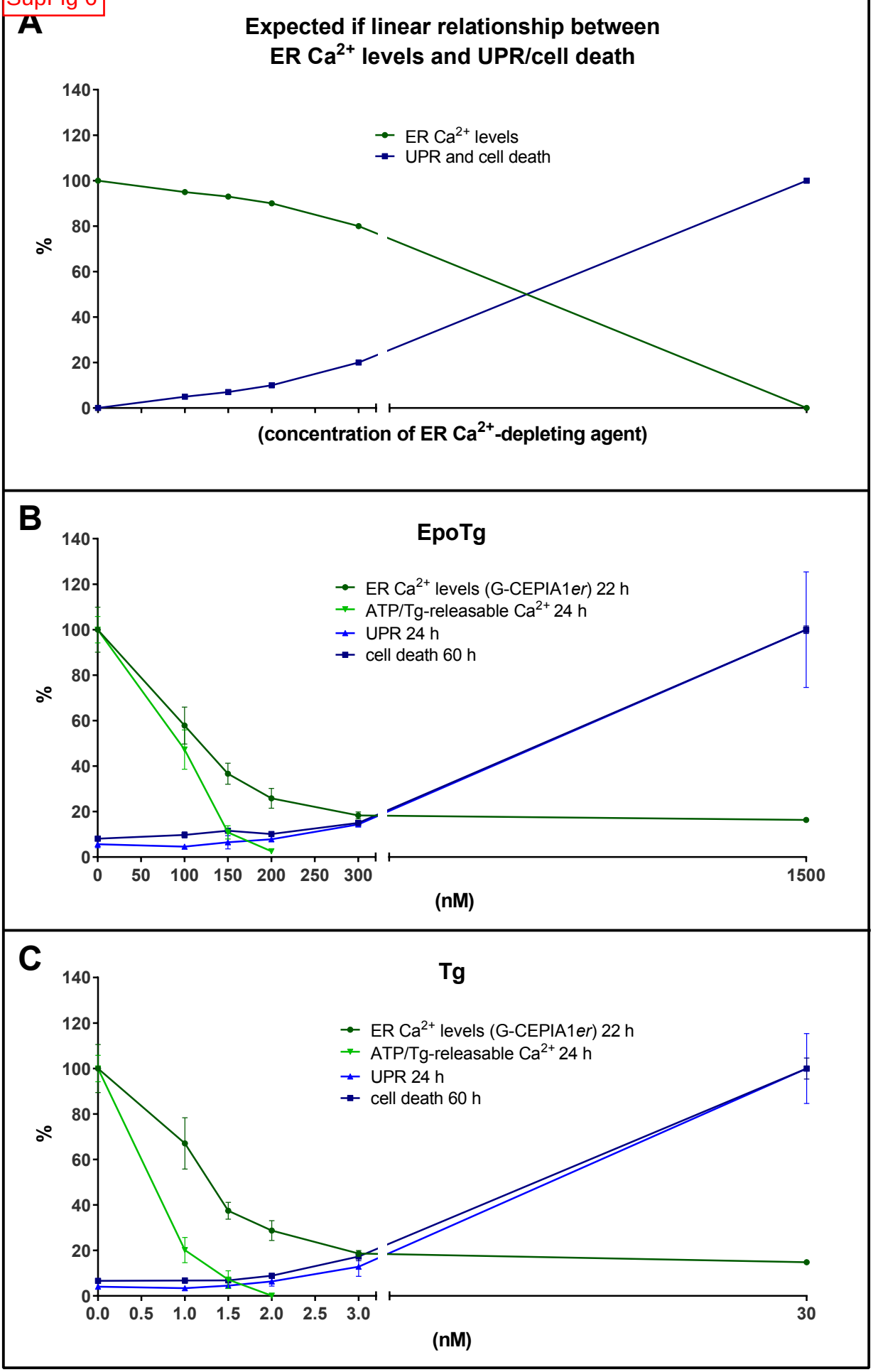
A
Expected if linear relationship between
ER Ca2+ levels and UPR/cell death
ER Ca2+ levels
UPR and cell death
%
(concentration of ER Ca2+-depleting agent)
B
EpoTg
ER Ca2+ levels (G-CEPIA1er) 22 h
ATP/Tg-releasable Ca2+ 24 h
UPR 24 h
cell death 60 h
%
(nM)
C
Tg
ER Ca2+ levels (G-CEPIA1er) 22 h
ATP/Tg-releasable Ca2+ 24 h
UPR 24 h
cell death 60 h
%
(nM)

SupFig 7

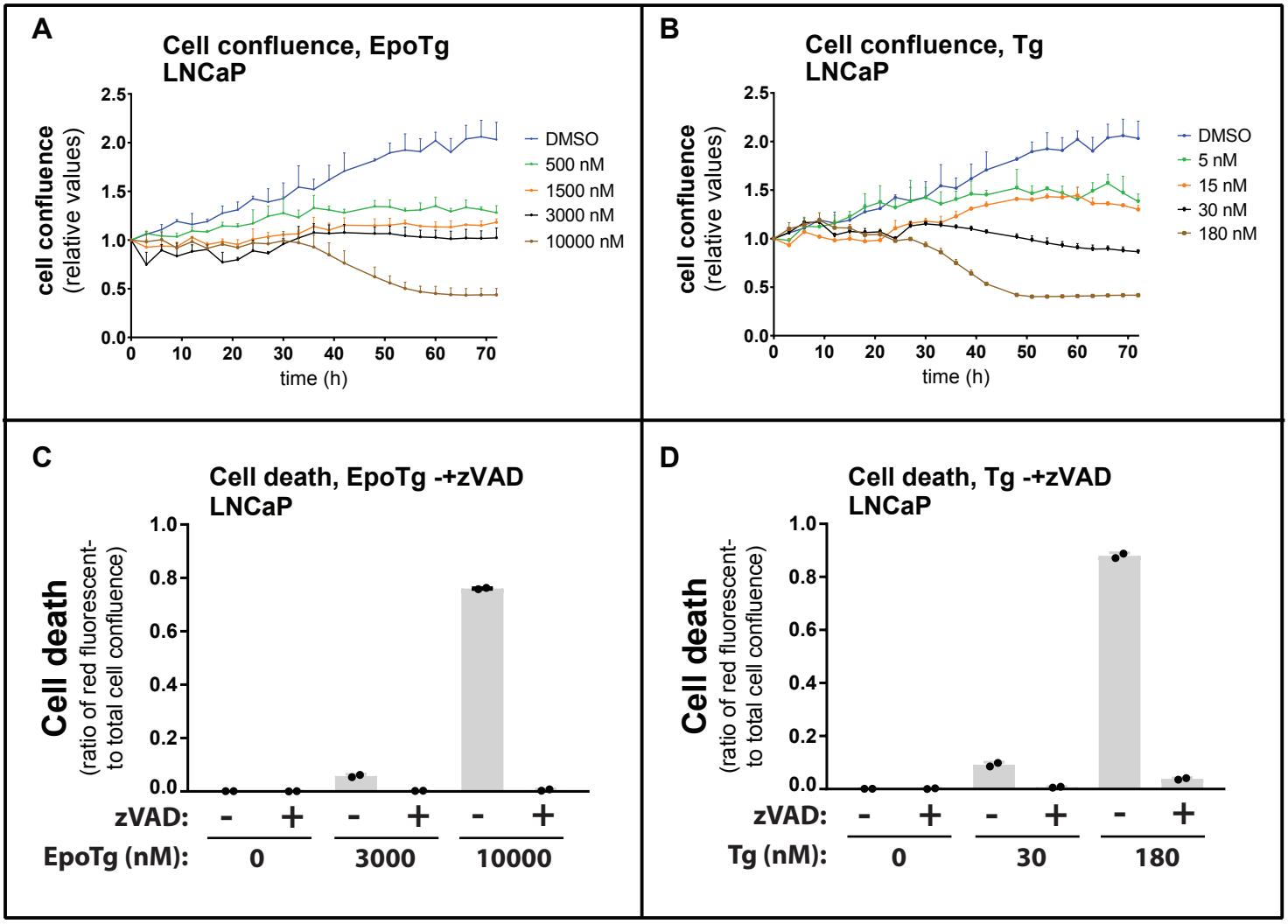
A
Cell confluence, EpoTg
LNCaP
cell confluence
(relative values)
time (h)
DMSO
500 nM
1500 nM
3000 nM
10000 nM
B
Cell confluence, Tg
LNCaP
cell confluence
(relative values)
time (h)
DMSO
5 nM
15 nM
30 nM
180 nM
C
Cell death, EpoTg -+zVAD
LNCaP
Cell death
(ratio of red fluorescent-
to total cell confluence)
zVAD:
EpoTg (nM):
0
3000
10000
D
Cell death, Tg -+zVAD
LNCaP
Cell death
(ratio of red fluorescent-
to total cell confluence)
zVAD:
Tg (nM):
0
30
180

SupFig 8

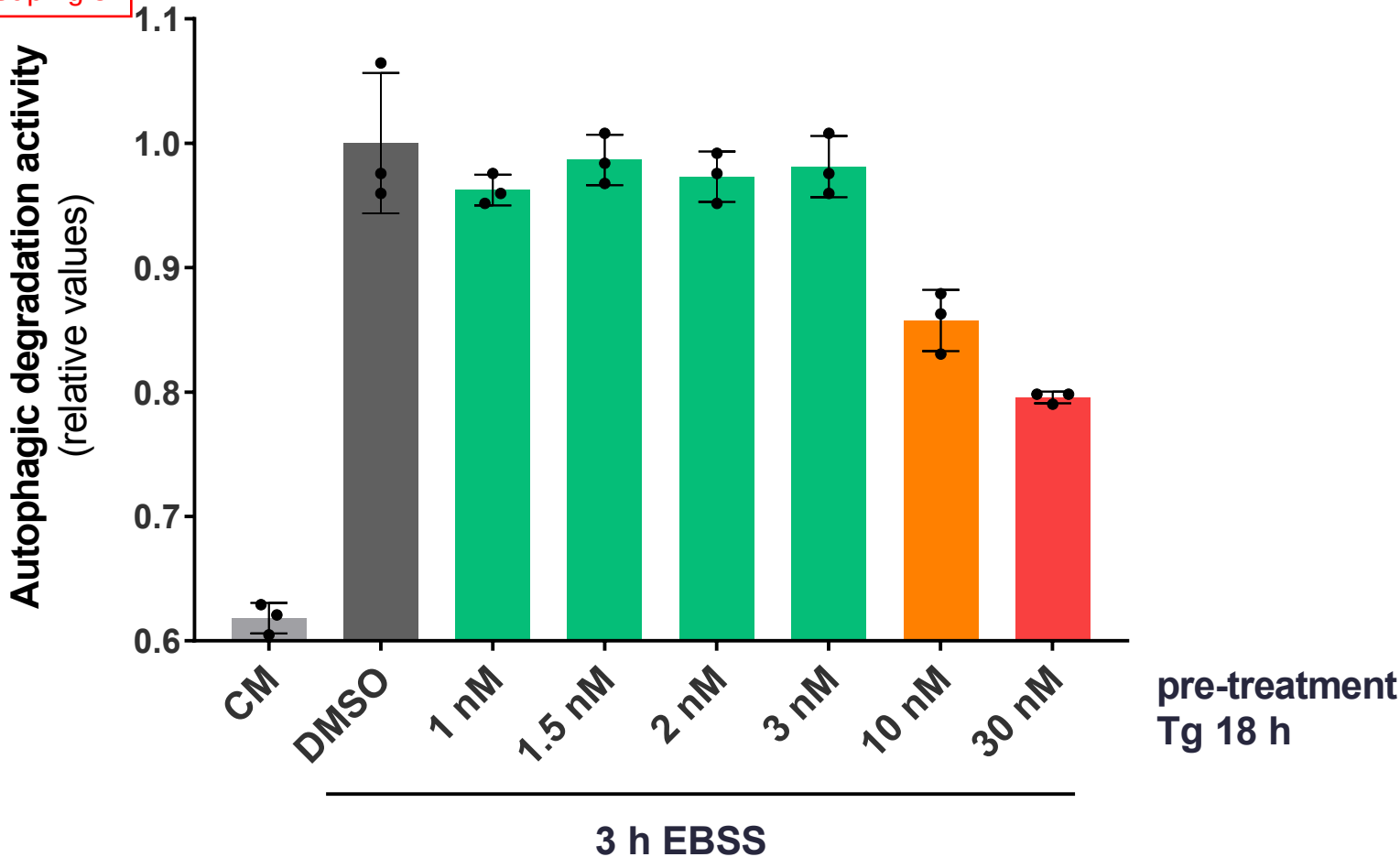
Autophagic degradation activity
(relative values)
1.1
1.0
0.9
0.8
0.7
0.6
CM
DMSO
1 nM
1.5 nM
2 nM
3 nM
10 nM
30 nM
pre-treatment
Tg 18 h
3 h EBSS